Published in final edited form as:
J Chem Neuroanat. 2007 July ; 33(4): 167–192.

Differential Localization of the GluR1 and GluR2 Subunits of the AMPA-type Glutamate Receptor Among Striatal Neuron Types in Rats

Y. P. Deng[1], **J. P. Xie**[1], **H. B. Wang**[1], **W. L. Lei**[1,2], **Q. Chen**[1], and **A. Reiner**[1]

1*Department of Anatomy and Neurobiology University of Tennessee Health Science Center Memphis, TN 38163*

2*Department of Anatomy Zhongshan Medical College, Sun Yat-Sen University Guangzhou, China*

Abstract

Differences among the various striatal projection neuron and interneuron types in cortical input, function, and vulnerability to degenerative insults may be related to differences among them in AMPA-type glutamate receptor abundance and subunit configuration. We therefore used immunolabeling to assess the frequency and abundance of GluR1 and GluR2, the most common AMPA subunits in striatum, in the main striatal neuron types. All neurons projecting to the external pallidum (GPe), internal pallidum (GPi) or substantia nigra, as identified by retrograde labeling, possessed perikaryal GluR2, while GluR1 was more common in striato-GPe than striato-GPi perikarya. The frequency and intensity of immunostaining indicated the rank order of their perikaryal GluR1:GluR2 ratio to be striato-GPe > striatonigral > striato-GPi. Ultrastructural studies suggested a differential localization of GluR1 and GluR2 to striatal projection neuron dendritic spines as well, with GluR1 seemingly more common in striato-GPe spines and GluR2 more common in striato-GPi and/or striatonigral spines. Comparisons among projection neurons and interneurons revealed GluR1 to be most common and abundant in parvalbuminergic interneurons, and GluR2 most common and abundant in projection neurons, with the rank order for the GluR1:GluR2 ratio being parvalbuminergic interneurons > calretinergic interneurons > cholinergic interneurons > projection neurons > somatostatinergic interneurons. Striosomal projection neurons had a higher GluR1:GluR2 ratio than did matrix projection neurons. The abundance of both GluR1 and GluR2 in striatal parvalbuminergic interneurons and projection neurons is consistent with their prominent cortical input and susceptibility to excitotoxic insult, while differences in GluR1: GluR2 ratio among projection neurons are likely to yield differences in Ca2+ permeability, desensitization, and single channel current, which may contribute to differences among them in plasticity, synaptic integration, and excitotoxic vulnerability. The apparent association of the GluR1 subunit with synaptic plasticity, in particular, suggests striato-GPe neuron spines as a particular site of corticostriatal synaptic plasticity, presumably associated with motor learning.

Keywords

striatum; AMPA receptors; AMPA subunits; glutamate; excitotoxicity; immunohistochemistry

Send correspondence to: Dr. Anton Reiner Department of Anatomy & Neurobiology University of Tennessee Health Science Center 855 Monroe Ave. Memphis, TN 38163 Phone: 901-448-8298 Fax: 901-448-7193 Email: areiner@utmem.edu

Introduction

The striatum contains diverse projection neuron and interneuron types, which differ in their connectivity, neurochemistry and roles in basal ganglia function. For example, four types of GABAergic medium-sized spiny projection neurons have been identified: 1) those containing enkephalin (ENK) that project to the external pallidal segment (GPe) and inhibit unwanted movements; 2) those containing substance P (SP) that project to the internal pallidal segment (GPi) and facilitate planned movements of trunk and limbs; 3) those containing SP that project to the substantia nigra pars reticulata (SNr) and facilitate planned movement of head and eyes; and 4) those containing SP that project to the substantia nigra pars compacta (SNc) and modulate the dopaminergic neurons projecting to the striatum (Albin et al., 1989;DeLong, 1990;Graybiel, 1990;Reiner and Anderson, 1990;Gerfen, 1992). Striato-GPe, striato-GPi and striato-SNr perikarya reside within the matrix compartment of striatum, while striato-SNc perikarya reside within the striosomal compartment (Graybiel, 1990;Reiner and Anderson, 1990;Gerfen, 1992). Striatal interneurons include: 1) large aspiny cholinergic neurons (Graybiel 1990;Gerfen, 1992;Kawaguchi et al., 1995;Bennett et al., 2000); 2) large aspiny neurons that contain GABA and parvalbumin (PARV) (Kita et al., 1990;Kawaguchi et al., 1995); 3) medium-sized aspiny neurons that contain GABA, somatostatin (SS), neuropeptide Y (NPY), and nitric oxide synthase (NOS) (Kawaguchi et al., 1995;Figueredo-Cardenas et al., 1996a); and 4) medium-sized aspiny neurons that contain GABA and calretinin (CALR) (Bennett and Bolam, 1993;Kubota et al., 1993;Kawaguchi et al., 1995;Figueredo-Cardenas et al., 1996b;Cicchetti et al., 1999,2000). While the roles of the SS+ and CALR+ interneurons are uncertain, cholinergic and PARV+ interneurons modulate striatal projection neurons (Kita et al., 1990;Kawaguchi, 1993;Kawaguchi et al., 1995;Koos and Tepper, 1999).

The striatal neuron types also differ in their vulnerability to neurodegenerative insults. For example, striatal projection neurons and PARV+ interneurons are vulnerable to Huntington's disease (HD), ischemia, and/or excitotoxicity, while cholinergic, SS+, and calretinergic striatal interneurons are resistant (Dawbarn et al., 1985;Ferrante et al, 1985,1987a,b;Beal et al., 1986,1991;Kowall et al., 1987;Reiner et al., 1988;Albin et al., 1990a,b;Chesselet et al., 1990;Hawker and Lang, 1990;Uemura et al., 1990;Bazzett et al., 1993;Figueredo-Cardenas et al., 1994,1997,1998;Richfield et al., 1995;Sapp et al., 1995; Cichetti and Parent, 1996; Cichetti et al., 1996, 2000;Meade et al., 2000). Although vulnerable as a group (Vonsattel et al., 1985;Vonsattel and DiFiglia, 1998), projection neurons differ from one another in their relative vulnerability, with striato-GPi neurons being least vulnerable and striato-GPe neurons most vulnerable (Reiner et al., 1988;Albin et al., 1990a,b;Figueredo-Cardenas et al., 1994;Richfield et al., 1995;Sapp et al., 1995;Glass et al., 2000;Meade et al., 2000;Deng et al., 2004).

Consistent with their functional differences and possibly their differential vulnerability to insults, striatal neuron types differ in the extent to which they receive cortical input. Striatal projection neurons, for example, receive a massive axospinous excitatory input from cerebral cortex (Somogyi et al., 1981;Gerfen, 1992), while cholinergic interneurons receive their major excitatory input from the parafascicular thalamic nucleus (Lapper and Bolam, 1992), and SS/NPY/NOS interneurons receive little cortical input (Aoki and Pickel, 1989;Vuillet et al., 1989). The fast response of striatal neurons to excitatory input is mediated primarily by α-amino-3-hydroxy-5-methyl-ioxazole-4-propionic acid (AMPA) type ionotropic glutamate receptors (Keinanen et al., 1990;Rogers et al., 1991;Petralia and Wenthold, 1992;Martin et al., 1993a,b;Sato et al., 1993;Bernard et al., 1996;Stefani et al., 1998). AMPA receptors are multimeric transmembrane proteins that are assembled from combinations of GluR1-GluR4 subunits (Hollmann and Heinemann, 1994), and subunit composition determines divalent ion permeability, rectification, single channel conductance, and ion channel kinetics (Jonas and Burnashev, 1995). The GluR1 and GluR2 subunits are the most abundant AMPA subunits in striatum (Stefani et al., 1998), and their relative abundance in a given neuron is of particular

importance, since AMPA receptors containing the Q/R edited GluR2 subunits are Ca2+ impermeable, show a linear current-voltage relationship (Hollmann et al., 1991;Burnashev et al., 1992), possess a smaller single-channel conductance, and desensitize and deactivate more slowly (especially in the flip isoform) than do GluR2-lacking AMPA receptors (Hollmann et al., 1991;Burnashev et al., 1992;Herlitze et al., 1993;Geiger et al., 1995;Angulo et al., 1997;Swanson et al., 1997;Washburn et al., 1997).

Thus, information on the localization of GluR1 and GluR2 in the different types of striatal neurons may provide insight into differences among them in synaptic integration of convergent cortical input, corticostriatal synaptic plasticity underlying motor learning, and excitotoxic vulnerability (Wilson, 1992,1995;Jonas et al., 1994;Jog et al., 1999;Song and Huganir, 2002;Van Damme et al., 2002;Seidenman et al., 2003). While prior immunohistochemical, in situ hybridization histochemical (ISHH), and single cell reverse transcription-polymerase chain reaction (RT-PCR) studies have examined the localization of AMPA subunits in striatal neurons, the relative frequency and abundance of GluR1 and GluR2 in the various striatal projection neuron and interneuron types has not been fully clarified (Tallaksen-Greene and Albin, 1994;Chen et al., 1996,1998;Bernard et al., 1997;Kwok et al., 1997). We thus used LM and EM immunolabeling to: 1) detail the percent of each major striatal projection neuron type and interneuron that contains GluR1 and GluR2; and 2) characterize relative GluR1 and GluR2 abundance in each.

Materials and Methods

Subjects

Twenty-nine adult male Sprague-Dawley rats (250-350gm; Harlan, Indianapolis, IN) were used to obtain the present data on the localization of GluR1 and GluR2 in striatal projection neurons and interneurons (nine in the studies using LM immunolabeling alone, twelve in the studies combining immunolabeling and retrograde labeling, and eight in the studies using EM immunolabeling). To identify striatal projection neuron types, two approaches were used: 1) retrograde labeling to distinguish types based on projection target; and 2) immunolabeling for calbindin or the mu opiate receptor to distinguish patch from matrix projection neurons. To identify interneurons, immunolabeling for type-specific markers was used. EM immunolabeling was used to characterize the cell-type specific localization of GluR1 and GluR2 to the spines of striatal projection neurons. All studies were in accordance with National Institutes of Health, Society for Neuroscience, and University of Tennessee policies on animal use, and every effort was made to minimize the numbers used.

RDA3k retrograde labeling of striatal projection neurons

Three primary types of striatal projection neurons have been identified in rodents, striato-GPe, striato-GPi and striatonigral (Kawaguchi et al., 1990;Reiner and Anderson, 1990)[1]. While the axons of the latter two collateralize to some extent in each other's target areas, they appear to be distinct types because: 1) they differ in the primary site of their collateralization, the GPi in the case of striato-GPi neurons and the nigra in the case of striatonigral neurons (Kawaguchi et al., 1990); and 2) they differ in their vulnerability to quinolinic acid and global ischemia (Figueredo-Cardenas et al., 1994;Meade et al., 2000). To retrogradely label these types, twelve adult rats were anesthetized with ketamine (0.33ml/500g) and xylazine (0.16ml/500g) and secured in a stereotaxic apparatus. RDA3k (tetramethylrhodamine dextran amine, 3000MW,

[1]In the present study we use the same terminology for rodents as commonly used in primates for the two subdivisions of the pallidum, as recommended by Paxinos and Watson (1998). Thus, the rodent globus pallidus is called the external part of globus pallidus (GPe), while the rodent entopeduncular nucleus is called the internal part of globus pallidus (GPi). This change simplifies discussions of similarities between primates and rodents.

Molecular Probes, Eugene, OR) dissolved in 0.1 M sodium citrate-HCl buffer (pH 3.0) was injected (0.2μl, 10%) bilaterally into GPe, GPi or SN (n=4, for each group) using a 1μl Hamilton syringe, at the following coordinates from the Paxinos and Watson (1998) stereotaxic atlas of the rat brain: 1) for GPe, AP −1.3mm, ML ±3.2mm, DV −6.5mm; 2) for GPi, AP −2.3mm, ML ±2.8mm, DV −8.0mm; and 3) for SN, AP −5.3mm, ML ±2.5mm, DV −8.5mm. The RDA3k injection was completed in 20 min and the syringe was left in place for another 5 min before withdrawal. The RDA3k-injected rats were allowed to survive for 5-7 days before being sacrificed (Reiner et al., 2000).

The injection site accuracy for the retrograde labeling cases was assessed by examining the needle track and injection site using an Olympus BH-2 fluorescence epi-illumination microscope (Fig. 1). Results for only the 12 rats with successful injections confined to the intended target and ample retrograde labeling are presented here, and in all twelve the injections were bilaterally accurate. These rats were used to determine the percentage of perikarya of these three projection neuron types that contain GluR1 or GluR2, as well as assess the GluR1 and GluR2 labeling intensities among them. Note that since striato-GPi and striatonigral neurons send a minor collateral into GPe (Kawaguchi et al., 1990;Wu et al., 2000), the RDA3k injection into GPe may have also labeled some striato-GPi or striatonigral neurons. A prior single-cell RT-PCR study of ours (Wang et al., 2006), however, indicates that no more than 25% of striatal neurons retrogradely labeled from GPe are striato-GPi or striatonigral neurons. Similarly, retrograde tracer injections into GPi might yield labeling of striatonigral neurons via their fibers of passage through the GPi, and retrograde tracer injection into nigra might yield labeling of striato-GPi neurons via their collaterals in the nigra (Kawaguchi et al., 1990;Wu et al., 2000). Prior studies suggest, however, that any such unintended labeling is not so extensive (about 20% labeled from GPi may be striatonigral and 20% from nigra may be striato-GPi) as to obscure trends for the population intended for retrograde labeling (Figueredo-Cardenas et al., 1994;Wang et al., 2006).

Fixation and Sectioning

The 12 RDA-injected rats, as well as 9 normal rats, were deeply anesthetized (1ml of 35% chloral hydrate, i.p.), and perfused transcardially with 100ml normal saline (0.9% NaCl), followed by 400ml of cold 4% paraformaldehyde, 0.1 M lysine-0.1 M sodium periodate in 0.1 M phosphate buffer (PB; pH 7.4). Brains were immediately removed and postfixed in the same fixative for another 4-6 h at 4°C. Brains were then cryoprotected overnight in 20% sucrose/10% glycerol at 4°C. Transverse brain sections (35 μm) were cut frozen on a sliding microtome.

Immunofluorescence Double-labeling

Immunofluorescence double-labeling was carried out on tissue from the nine normal rats, as described previously (Chen, et al., 1996;Fusco, et al., 1999;Meade, et al., 2002;Deng et al., 2006). In brief, free-floating brain sections were incubated in a cocktail containing two primary antibodies, one directed against either GluR1 or GluR2 (Table 1), and the other against a marker for a given striatal neuron type. The dilutant used for all antibodies was 0.1M PB containing 0.3% Triton X-100 and 0.01% sodium azide (PBTX). To detect GluR1, a rabbit polyclonal antibody directed against GluR1 was used. To detect GluR2, a monoclonal antibody raised against amino acids 175-430 of rat GluR2, which is near the N-terminus and unique to this subunit, was used. The working dilutions, host species, sources, and references indicating specificity and efficacy of the anti-GluR1 and GluR2 are shown in Table 1.

In our studies using the rabbit polyclonal anti-GluR1, we identified striatal neuron types immunohistochemically using: 1) a mouse monoclonal anti-calbindin D28k (CALB) antibody to detect CALB-containing matrix projection neurons; 2) a guinea pig polyclonal anti-mu opiate receptor (MOR) antibody to identify the striatal patch compartment; 3) a mouse

monoclonal anti-CALR antibody to recognize the medium-sized GABAergic CALR-containing aspiny striatal interneurons; 4) a goat polyclonal anti-ChAT antibody to label the large cholinergic aspiny striatal interneurons; 5) a mouse monoclonal anti-PARV antibody to label the large GABAergic PARV-containing aspiny striatal interneurons; and 6) a mouse monoclonal anti-somatostatin (SS) antibody to label striatal SS/NPY/NOS interneurons (Figueredo-Cardenas et al., 1996a). The working dilutions, host species, sources, and references indicating specificity and efficacy for each of these antisera are shown in Table 1.

To identify striatal neuron types in the double-label immunofluorescence studies using the mouse monoclonal anti-GluR2, we needed to use a different set of antisera for the type specific markers: 1) a rabbit polyclonal anti-CALB antibody to detect CALB-containing matrix projection neurons; 2) a rabbit polyclonal anti-MOR antibody to identify the patch compartment; 3) a rabbit polyclonal anti-CALR antibody to recognize the medium-sized GABAergic CALR-containing aspiny striatal interneurons; 4) a rabbit polyclonal anti-ChAT antibody to label the large cholinergic aspiny striatal interneurons; 5) a rabbit polyclonal anti-PARV antibody to label the large GABAergic PARV-containing aspiny striatal interneurons; and 6) a rabbit polyclonal anti-SS antibody to label striatal SS/NPY/NOS interneurons. The working dilutions, host species, sources, and references indicating specificity and efficacy for each of these antisera are shown in Table 1. The pairs of antibodies directed against the same neuron type-specific markers were comparable in their sensitivity and selectivity, as directly determined by us in single- and double-label studies for each pair of antibodies against the same neuron marker.

After 72 h incubation in the primary antibody cocktail at 4°C with gentle agitation, the secondary antibody incubations were carried out. The sections for co-localization of GluR1 and CALB, MOR, CALR, PARV or SS were incubated in a secondary antisera mixture that contained an Alexa 488-conjugated goat anti-rabbit IgG (to detect GluR1) and an Alexa 594-conjugated goat anti-mouse (to detect neuron type) (Molecular Probes) for 1 h at room temperature. For studies involving double-labeling with rabbit anti-GluR1 and guinea pig anti-MOR, Alexa 488-conjugated donkey anti-rabbit IgG and Alexa 594-conjugated donkey anti-guinea pig IgG were used, respectively. For studies involving double-labeling with rabbit anti-GluR1 and goat anti-ChAT, Alexa 488-conjugated donkey anti-rabbit IgG and Alexa 594-conjugated donkey anti-goat IgG were used, respectively. After primary antiserum incubation, the sections for co-localization of GluR2 and CALB, MOR, CALR, ChAT, PARV or SS were incubated in a secondary antisera mixture that contained an Alexa 488-conjugated goat anti-mouse IgG (to detect GluR2) and an Alexa 594-conjugated goat anti-rabbit IgG (to detect neuron type) (Molecular Probes) for 1 h at room temperature. All sections were thereafter washed with 0.1M PB, mounted on gelatin-coated slides, and coverslipped with ProLong® antifade medium (Molecular Probes). The Alexa dyes are brighter and more fade-resistant than are fluorescein or rhodamine (Panchuk-Voloshina et al., 1999), the latter of which had been used in prior immunofluorescence studies of GluR1 and GluR2/3 localization in rat striatum (Tallaksen-Greene and Albin, 1994;Chen et al., 1996;Bernard et al., 1997;Kwok et al, 1997). Moreover, the ProLong antifade medium is more effective at preventing fading of fluorescence than the coverslipping media used in prior studies (Ono et al., 2001). For these reasons, GluR1 and GluR2 detection was more sensitive than in prior studies of their striatal localization.

Immunofluorescence Single-labeling Combined with Retrograde Labeling

Immunofluorescence single-labeling was carried out on tissue from the twelve rats with RDA3k retrograde labeling to localize GluR1 and GluR2 in striatal neurons projecting to specific targets. For these studies, free-floating brain sections were incubated in the antibody directed against GluR1 or GluR2 (Table 1). After a 72 h incubation in the primary antibody at 4°C with gentle agitation, the sections for GluR1 detection were incubated for 1 h at room

temperature in Alexa 488-conjugated goat anti-rabbit IgG (Molecular Probes), while those for GluR2 detection were incubated for 1 h at room temperature in Alexa 488-conjugated goat anti-mouse IgG (Molecular Probes). Thereafter, the sections were washed with 0.1M PB, mounted on gelatin-coated slides, and coverslipped with antifade medium (Molecular Probes).

Quantification of Frequency of GluR1 or GluR2 in Striatal Neuron Types

The percentage of each type of striatal perikarya containing GluR1 or GluR2 was determined from images collected using a Bio-Rad MRC-1000 confocal laser scanning microscope (CLSM). In the immunofluorescence double-label studies in which striatal neuron types were identified by immunolabeling for type-specific markers, sections from each of 4-5 rats were used to determine the frequency of GluR1 or GluR2 perikaryal localization for each neuron type. For each rat, sections from rostral, middle and caudal striatum were analyzed, with separate counts carried out on the dorsomedial, dorsolateral, ventromedial, and ventrolateral quadrants for each side of the brain. For GluR1 frequency assessment, CLSM images were collected using a 40× oil immersion objective, and labeled perikarya were identified by subsequent analysis of these images. About 1-3 cholinergic, somatostatinergic or calretinergic interneurons, about 20 parvalbuminergic interneurons and about 15 calbindinergic projection neurons in each quadrant were randomly chosen for GluR1 frequency assessment. For GluR2 assessment, CLSM images were scanned and captured using a 40× oil immersion objective, and viewed on a computer monitor. The double labeling frequencies for GluR2 were assessed on the monitor as they were captured by 2 viewers working together (YPD and JPX), and some of the GluR2 images were saved for intensity measurement. About 5-20 interneurons (cholinergic, parvalbuminergic, somatostatinergic or calretinergic) and 40 projection neurons (calbindinergic) in each quadrant were randomly chosen for GluR2 frequency assessment. Because labeling of striatal neuropil was light to moderate for GluR2 and GluR2 perikaryal labeling relatively intense for most striatal neurons, the perikarya labeled for GluR2 stood out clearly against the background, and could thereby readily be identified and counted in the displayed images by the viewers. By contrast, neuropil labeling was more prominent for GluR1 and perikaryal labeling typically lighter, at least for medium-sized neurons. As a result, identification of GluR1+ striatal perikarya was less clear. For this reason, we used computer-assisted analysis of the captured GluR1 images, using NIH Image, to identify striatal perikarya immunolabeled for GluR1. We used a standard that a perikaryon had to be at least 10 grayscale units higher in intensity than the nearby unlabeled background to be considered as positively immunolabeled for GluR1. Because of the more time-consuming nature of this approach, fewer perikarya were analyzed for GluR1 than GluR2.

For characterization of GluR1 and GluR2 frequency in retrogradely labeled striatal projection neurons (striato-GPe, striato-GPi, striatonigral), 50-100 retrogradely labeled neurons from three to six sections were randomly analyzed in the four animals for each type of retrogradely labeled projection neuron and each of GluR1 and GluR2 (with approximately 25-50 retrogradely labeled neurons per side counted in each animal). Since the location of retrogradely labeled neurons depended on the part of the projection target injected, equal numbers of retrogradely labeled neurons could not be counted in each striatal quadrant for each retrograde labeling case.

Quantification of GluR1 or GluR2 Immunolabeling Intensity in Striatal Neuron Types

To assess relative differences among striatal neuron types, as defined by immunolabeling or retrograde labeling, in perikaryal GluR1 or GluR2 levels, we measured their GluR1- or GluR2-immunolabeling intensities. The immunolabeling intensities were quantified in images sequentially collected using the Bio-Rad MRC-1000 CLSM. Each image consisted of three consecutive stacked z series, taken at 1μm intervals. To standardize the labeling represented in the images, a fixed setting for scan head pinhole aperture, laser intensity, gain, brightness/

contrast level, and image file size was used. The intensity of GluR1 or GluR2 labeling in the perikaryal cytoplasm (i.e. excluding the nucleus) was measured using NIH Image (Version 1.62) by outlining the cytoplasmic domain of individual neurons and determining their labeling intensity using the particle analysis function, minus background labeling intensity as determined from a nearby unlabeled region of striatal neuropil. The intensity was expressed on an inverted 0-255 grayscale, with 0 representing black (as observed over unlabeled fiber bundles) and 255 representing white (maximally intense labeling). The approach we used allowed us to characterize the relative GluR immunolabeling intensity for a comparably thick slice through the perikaryal cytoplasm of each neuron type examined. This, in turn, allowed us to rank order relative labeling intensities, even in the absence of calibration of the protein level associated with a particular intensity.

The relative GluR1 and GluR2 intensities were assessed in either of three specific within-set comparisons: 1) among CALB+ matrix projection neurons and various interneurons detected by immunolabeling; 2) among retrogradely labeled projection neurons; and 3) between perikarya of patch and matrix, with the compartments distinguished by CALB immunolabeling or MOR immunolabeling. Within each comparison, the tissue was processed as a set so that staining variation due to procedural variation was minimized for that comparison. Across all comparisons, dilution and incubation time for the GluR1 or GluR2 antibodies and secondary antibodies were the same. To quantify GluR1 intensity among CALB+ matrix projection neurons and striatal ChAT+, PARV+, CALR+ interneurons, 100 perikarya for CALB+ projection neurons, 100 perikarya each for ChAT+ and PARV+, and 96 perikarya for CALR + interneuron were collected in 4 animals (25 per animal) from tissue double-immunolabeled for GluR1 and the cell type marker. Since not many SS+ neurons were found to contain GluR1 immunolabeling, only 20 of them were collected for intensity quantification. To quantify GluR2 intensity among CALB+ matrix projection neurons and striatal ChAT+, PARV+, SS+, CALR+ interneurons, 100 perikarya each for CALB+ projection neurons and PARV+ interneurons (50 per animal) and 50 for each type of interneuron (ChAT+, SS+, and CALR+) were collected in 2 animals (25 per animal) from tissue double-immunolabeled for GluR2 and the cell type marker. Note that because it was more laborious to identify GluR1+ perikarya than GluR2+ perikarya, we needed to analyze images from more animals for GluR1 than for GluR2 to obtain a sufficient number for our pool for a given neuron type, especially for projection neuron.

To quantify GluR1 or GluR2 perikaryal intensity between patch and matrix compartments, 100 medium-sized neurons in the CALB-positive matrix and 100 in CALB-negative patches from sections double-labeled for GluR and CALB (25 per rat in 4 rats for GluR1; 50 per rat in 2 rats for GluR2) were captured, as were 50 medium-sized neurons within the MOR-negative matrix and 50 from MOR-positive patches from sections double-labeled for GluR and MOR (25 per rat in 2 rats for both GluR1 and GluR2). For the patch versus matrix comparisons, since 90-95% of the striatal neurons are medium-sized spiny projection neurons, measuring only medium-sized neurons in MOR-rich, CALB-poor patch or MOR-poor CALB-rich matrix largely restricts the measurement to projection neurons, i.e. it excludes cholinergic and PARV+ interneurons (which are large) but may include SS+ and CALR+ interneurons (which are medium-sized). Since each of the latter two types represents 1% or less of all striatal neurons (Figueredo-Cardenas et al., 1996a,1996b), inadvertent inclusion of them is unlikely to significantly affect the assessment of GluR perikaryal labeling intensity.

For the comparisons among striato-GPe, striato-GPi, and striatonigral projection neurons, 100 GluR1+ cells and 120 GluR2+ cells for each projection neuron type from 4 animals were collected and analyzed (25 per animal for GluR1, 30 per animal for GluR2).

Statistical Analysis

The percent of each neuron type labeled for GluR1 or GluR2 was calculated in either of two ways: 1) as the mean of the GluR perikaryal localization percentages per animal for that cell type; and 2) as the percent of that neuron type labeled for GluR with data for that cell type pooled across animals. The percent colocalization for GluR per cell type was nearly identical by these two approaches, and the frequency values presented in this paper are the group means. To statistically assess if there were differences in GluR1 or GluR2 intensity among projection and interneuron types, and among projection neurons defined by retrograde labeling, one-way ANOVA with post-hoc analysis (Fisher's PLSD) was used. Pooled data for two-four animals per cell type were analyzed for the immunolabeled striatal neuron types, while pooled data for four animals were used for each of the retrogradely labeled neuron types. A paired student's t-test (two-tailed) was used to compare GluR intensity between patch and matrix compartments in the CALB and MOR immunolabeled tissue for perikaryal data pooled from two rats.

Electron Microscopic Immunohistochemical Studies

To characterize possible differences in the localization of GluR1 and GluR2 to the spines and dendrites of striatal projection neurons, we immunolabeled striatal sections for GluR1, GluR2, or GluR2/3 for electron microscopy as described previously (Chen et al., 1998). For these EM studies, we used anti-GluR2/3 as well as the anti-GluR2 to assess the ultrastructural localization of GluR2 because the anti-GluR2/3 immunolabels the striatal neuropil more robustly than does the anti-GluR2. While the anti-GluR2/3 recognizes an epitope common to rat GluR2 and GluR3 (Wenthold et al., 1992), and thus does not distinguish between GluR2 and GluR3, GluR3 is much rarer than GluR2 in rat striatum (Stefani et al., 1998). Thus, in light of its apparently greater sensitivity than the anti-GluR2 for neuropil labeling, we believed the anti-GluR2/3 could provide useful corroboration of the EM findings with the anti-GluR2 on GluR2 localization to spines and dendrites in striatum.

Eight rats were transcardially perfused with a fixative containing 15% saturated picric acid, 0.6% glutaraldehyde, and 3.5% paraformaldehyde in 0.1M PB (pH7.2). After perfusion, the brains were post-fixed overnight in the same fixative but without glutaraldehyde, and then cut on a vibratome into 50μm coronal sections. To optimize immunostaining, tissue was treated with 1% sodium borohydride and then with a 5% NHS (normal horse serum) blocking solution. The tissue was next incubated in primary antiserum against GluR1, GluR2 or GluR2/3, diluted with 5% NHS in PBTX, and the peroxidase-antiperoxidase (PAP) method used to visualize the glutamate receptor subunit localization with diaminobenzidine tetrahydrochloride (DAB), as detailed in our prior studies (Reiner et al., 2003;Lei et al., 2004). The immunolabeled sections for electron microscopic studies were post-fixed in 2% OsO_4 in cacodylate buffer (pH 7.2), dehydrated, impregnated with 1% uranyl acetate in 100% alcohol, and finally infiltrated with Spurr's resin (Electron Microscopy Sciences, Fort Washington, PA). The sections were then flat-embedded on microslides pretreated with liquid releasing factor (Electron Microscopy Sciences). Small rectangular areas were cut from the dorsolateral somatomotor striatum. We focused our attention on dorsolateral striatum so as to minimize inclusion of striosomal neurons, which project to pars compacta of the nigra (Gerfen, 1992) and are scarce in dorsolateral striatum (Gerfen, 1992;Desban et al., 1993). Since immunolabeling in striosomes was higher for GluR1 than in the matrix, we were additionally able to select samples from the matrix compartment for GluR1 by their lesser labeling intensity. Section samples were glued to carrier blocks, and thin and ultrathin sections cut with a Reichert ultramicrotome, mounted on mesh grids, and stained with lead citrate and uranyl acetate using an LKB Ultrostainer. To obtain the images containing optimal labeling, ultrathin sections from the surface of the block were chosen for EM image capture. The sections were examined with a Jeol 2000 electron microscope. Images of the striatum containing immunolabeled structures (perikarya, dendrites and spines) were randomly captured at 7,500X – 35,000X magnification. The frequency of

labeled spines and dendrites was determined from these images. The diameter of asymmetric synaptic terminals ending on immunolabeled spines was determined at their widest point parallel to the postsynaptic density. Spines were identifiable by their size, continuity with dendrites, prominent postsynaptic density, and/or the presence of spine apparatus (Reiner et al., 2003;Lei et al., 2004).

Results

Distribution of GluR1 and GluR2 in Striatum

GluR1-immunoreactive perikarya were abundant and widespread in rat striatum (Fig. 2A), as were GluR2-imunoreactive perikarya (Fig. 2B). The GluR1-immunoreactive perikarya were, however, somewhat less common than were the GluR2-immunoreactive perikarya. The labeled perikarya for both GluR1 and GluR2 included those of medium-sized neurons (a few indicated by arrows in panels A and B of Fig. 2) and large neurons (a few indicated by arrowheads in panels A and B of Fig. 2). By far, the most common GluR1-immunoreactive neuron type and the most common GluR2-immunoreactive neuron type had a medium-sized perikaryon, was moderately labeled, and had a uniform striatal distribution. By their size, frequency and distribution, these labeled perikarya appeared to belong to striatal projection neurons. One additional but low frequency group of GluR1-immunolabeled striatal neurons, whose members possessed a medium-sized to large perikaryon, was distinguished by the fact that their perikarya were much more intensely labeled than were those of any other striatal neurons (indicated by arrowheads in Fig. 2A). These neurons were sparsely but uniformly distributed in the striatum. Additional rare, large, moderately GluR1+ neuronal perikarya were also present. By contrast, perikaryal labeling among the different-sized striatal neurons was of more uniform intensity for GluR2 (Fig. 2B). Labeling in perikarya for GluR2 was typically confined to the cytoplasm, with nuclei unlabeled, and no evident dendritic labeling. Immunolabeling of medium-sized neurons for GluR1 was also typically confined to their cytoplasm, but perikarya and proximal dendrites both were immunolabeled in the case of the intensely GluR1-immunolabeled neurons with medium-sized to large perikarya (Fig. 2A). The high labeling intensity in this latter neuron type tended to obscure the nucleus.

Distinct neuropil immunolabeling was evident for GluR1 throughout striatum, but many scattered patches of more intense neuropil and perikaryal labeling for GluR1 were evident as well. These GluR1-immunolabeled patches resembled striosomes in their size and distribution, and examination of adjacent sections immunolabeled for MOR showed that these GluR1-rich patches tended to coincide with MOR-rich patches (Fig. 2C, D). Thus, the striosomal compartment tended to be more enriched than the matrix striatal compartment in GluR1. By contrast, immunolabeling of the striatal neuropil was light to moderate for GluR2 (Fig. 2B), and there was no prominent regional variation or patchiness in the frequency of GluR2-immunolabeled perikarya, their labeling intensity, or in the neuropil labeling intensity for GluR2. Thus, there appeared to be no major difference in GluR2 localization between striosomal and matrix compartments of striatum.

Frequency of GluR1 and GluR2 in Striatal Neuron Types

Striatal Projection Neurons—In our studies of GluR1 and GluR2 localization to striatal projection neuron perikarya, we used two approaches to identify striatal projection neurons: 1) immunolabeling for calbindin to identify matrix compartment projection neurons; and 2) retrograde labeling to distinguish types based on projection target. The former approach (in conjunction with separate analysis of interneuron immunolabeling) allowed us to distinguish between striatal projection neurons and interneurons, while the latter allowed us to distinguish among striatal neurons projecting to different targets. Tissue immunolabeled for calbindinergic striatal projection neurons was double-immunolabeled for detection of GluR1 or GluR2. In the

case of the retrograde labeling studies, immunofluorescence single-labeling for GluR1 or GluR2 was carried out on tissue from the twelve rats with RDA3k retrograde labeling. In four of these rats, striatal neurons were retrogradely labeled from GPe, in four others striatal neurons were retrogradely labeled from GPi, and in yet four others striatal neurons were retrogradely labeled from the substantia nigra. The RDA3k injections were targeted bilaterally for each particular striatal projection area, and in all twelve rats studied the injections were bilaterally accurate.

Immunofluorescence labeling for GluR1 or GluR2 revealed that all projection neurons, regardless of whether calbindin immunolabeling or RDA3k retrograde labeling was used to identify them, contained GluR2, but not all contained GluR1 (Figs. 3-5; Tables 2, 3). For example, all CALB+ striatal projection neurons of the matrix compartment showed an overlap of their uniform perikaryal Alexa 594 (red) immunolabeling for CALB (Fig 3D) with the Alexa 488 (green) cytoplasmic ring of GluR2 immunofluorescence (Fig. 3E), which in the merged CLSM images (Fig. 3F) was evident as a yellow-orange ring (Table 2). Note that some medium-sized and large neurons in this tissue were GluR2-only (i.e. exhibited a green-only cytoplasmic ring of immunofluorescence in the merged CLSM images) (Fig. 3C). This observation is consistent with the findings that not all striatal projection neurons contain immunohistochemically detectible CALB in rodents (Wang et al., 2006), nor do large striatal interneurons (Gerfen and Wilson, 1996). In contrast to the ubiquity of GluR2 in calbindinergic striatal neurons, not all striatal projection neurons of the matrix compartment, as identified by their uniform perikaryal Alexa 594 (red) immunolabeling for CALB (Fig 3A), also showed an Alexa 488 (green) cytoplasmic ring of GluR1 immunofluorescence (Fig. 3B). While the majority of striatal CALB+ neurons in this tissue showed an overlap of red perikaryal immunofluorescence for CALB with the green cytoplasmic ring of immunofluorescence for GluR1, which in the merged CLSM images was evident as a yellow-orange ring, many did not (Fig. 3C). Counts of GluR1 frequency among CALB-immunolabeled perikarya revealed that only 61.9% of CALB+ perikarya contained GluR1 (Table 2). Note that, as for GluR2, some medium-sized and large neurons in this tissue were GluR1-only (i.e. exhibited a green-only cytoplasmic ring of immunofluorescence in the merged CLSM images) (Fig. 3C). Again, this reflects the findings that not all striatal projection neurons contain detectible CALB in rodents (Wang et al., 2006), and large striatal interneurons lack CALB as well (Gerfen and Wilson, 1996). In particular, the large, intensely GluR1+ perikarya did not label for CALB.

A similar pattern of results was obtained for striatal projection neurons identified by retrograde labeling with RDA3k. For example, not all retrogradely labeled striatal projection neurons, as identified by their uniform perikaryal RDA3k (red) labeling (Fig 4A, D, G), also contained an Alexa 488 (green) cytoplasmic ring of GluR1 immunofluorescence (Fig. 4B, E, H). This was true for striatal projection neurons retrogradely labeled from each of the three target areas. While the majority of RDA3k+ striatal projection neurons showed an overlap of red perikaryal immunofluorescence for RDA3k with the green cytoplasmic ring of immunofluorescence for GluR1, which in the merged CLSM images was evident as a yellow-orange ring, many did not (Fig. 4C, F, I). Nonetheless, counts of GluR1 frequency in retrogradely labeled perikarya from each target area revealed some slight differences in GluR1 frequency among the three populations (Table 3). For example, GluR1 was most prevalent among striatal neurons retrogradely labeled from GPe (71.6%), next most prevalent among those labeled from the nigra (62.2%), and least prevalent among those labeled from the GPi (53.4%). Note that since about 25% of striatal neurons retrogradely labeled from GPe are striato-GPi/nigral neurons labeled via their slight intra-GPe collateral (Wang et al., 2006), and since we found GluR1 frequency to be only 50-60% among striato-GPi/nigral neurons, it seems likely that GluR1 frequency among true striato-GPe neurons is somewhat higher than the 71.6% shown in the table for neurons labeled from GPe. Similarly, striatal neurons labeled from GPi include some striatonigral neurons labeled via their axon passing through GPi, and striatal neurons labeled

from the nigra include some striato-GPi neurons labeled via their collateral to the nigra. Thus, the GluR1 frequency for true striato-GPi neurons may be lower than the value shown for neurons labeled from GPi, and the GluR1 frequency for true striatonigral neurons may be higher than the value shown for neurons labeled from the nigra. Finally, note that since the RDA3k injections selectively labeled only striatal neurons of the type projecting to the site of the RDA3k injection, only a subset of striatal projection neurons were labeled in the striatum following any given injection. As a consequence, many medium-sized GluR1+ striatal neurons were evident that were devoid of retrograde labeling. These presumably represented projection neurons sending their axons elsewhere than to the region targeted by the RDA3k injection. Nonetheless, the intensely GluR1+ striatal perikarya were never observed to be retrogradely labeled in any animal.

As true in the studies in which we used CALB immunolabeling to mark striatal projection neurons, GluR2 was present in all retrogradely labeled striatal projection neuron perikarya, regardless of the target of the RDA3k injection (Fig. 5; Table 3). Thus, for all striatal perikarya labeled from GPe (Fig. 5A), GPi (Fig. 5D), or SN (Fig. 5G), the images of the GluR2 immunolabeling (Fig. 5B, E, H) revealed that the red perikaryal labeling for RDA3k overlapped the Alexa 488 (green) immunolabeling for GluR2, which in the merged CLSM images was evident as a yellow-orange ring (Fig. 5C, F, I). Again, since the RDA3k injections selectively labeled only striatal neurons of the type projecting to the site of the RDA3k injection, only a subset of striatal projection neurons were labeled in the striatum following any given injection. As a consequence, many medium-sized GluR2+ striatal neurons were evident that were devoid of retrograde labeling. These presumably represented projection neurons sending their axons elsewhere than to the region targeted by the RDA3k injection. Nonetheless, large GluR2+ striatal perikarya were never observed to be retrogradely labeled.

Striatal Interneurons—Immunofluorescence double-labeling was used to determine the extent to which GluR1 and GluR2 were present in the perikarya of each of the four main types of striatal interneurons. All of the PARV+ perikarya (which represent the medium-sized to large GABAergic interneurons of striatum), as revealed by their intense perikaryal Alexa 594 (red) immunolabeling for PARV (Fig. 6A), were rich in GluR1 (Table 2), as shown by their intense perikaryal Alexa 488 (green) immunolabeling for GluR1 (Fig. 6B). The perikaryal double-labeling was evident by CLSM as yellow-orange signal in much or all of the PARV-immunolabeled perikarya in the merged images (Fig. 6C). As found in previous studies (Tallaksen-Greene and Albin, 1994;Chen et al., 1996), the PARV+ interneurons largely accounted for the intensely GluR1+ neurons observed in our GluR1 single-labeling studies (Figs. 2A, 6A-C). For the other three interneuron types, GluR1 immunolabeling was more rare and much less intense than it was for the PARV+ interneurons (Figs. 7-9; Table 2). The frequency ranged from a high of 68.9% in ChAT-immunoreactive neurons (Fig. 7A-C), to a low of 14.8% for SS+ perikarya (Fig. 8A-F), to 51.2% of CALR+ interneuron perikarya (Fig. 9A-F).

In contrast to its ubiquity in striatal projection neurons, immunofluorescence double-labeling showed that GluR2 was present in only a fraction of each striatal interneuron type (Table 2; Figs. 6-9). For example, 73.2% of PARV+ perikarya possessed GluR2, and typically the GluR2 labeling intensity was moderate (Fig. 6D-I). By contrast, analysis of the CLSM images for ChAT (Fig. 7D-F) and SS (Fig. 8G-L) revealed that only about half of striatal cholinergic interneuron perikarya (55.4%) and about half of striatal somatostatinergic interneuron perikarya (51.8%) possessed GluR2 (Table 2). GluR2 was even less common in striatal CALR + perikarya (Fig. 9G-L), being present in only 33.0% (Table 2).

Patch versus Matrix—Our immunofluorescence double-label studies, using CALB (Fig. 10A, G) or MOR (Fig. 10D, J) to distinguish the patch and matrix compartments, showed that

both striatal compartments contained GluR1+ (B, C, E, F) and GluR2+ perikarya (Fig. 10H, I, K, L). We could not, however, quantify the percent of patch versus matrix neurons labeled for GluR1 or GluR2, because doing so would have required triple-labeling (one marker for the patch-matrix distinction, one to label all striatal neurons, and one to label the given GluR), and a compatible trio of antibodies was not available. Since the vast majority of striatal perikarya are projection neurons, however, the vast majority of perikarya in the MOR+/CALB− striosomes or the MOR−/CALB+ matrix compartment must be projection neurons. Given that we found that all projection neuron types identified by retrograde labeling contain GluR2 (Table 3; Fig. 5), a difference between patch and matrix compartments in the perikaryal frequency for GluR2 in projection neurons seems unlikely. The specific observation that all retrogradely labeled striatonigral neurons, which include matrix striato-SNr and patch striato-SNc neurons (Wang et al., 2006), contained GluR2 lends further support to the view that all striosomal and matrix projection neurons must contain GluR2. In light of the higher immunolabeling intensity for GluR1 in striosomes than in the matrix compartment (Figs. 2, 10), however, it is possible that striosomal neurons more commonly contain GluR1 than do matrix neurons.

GluR1 and GluR2 Intensity in Striatal Neuron Types

Striatal Projection Neurons and Interneurons—Qualitative assessments of the immunofluorescence double-labeled tissue suggested variation among striatal neuron types in the intensity of the perikaryal immunolabeling for GluR1 and GluR2. We therefore measured the labeling intensity for GluR1 and GluR2 among the various striatal neuron types examined. For immunolabeled striatal perikarya (i.e. excluding GluR-negative neurons from the calculation of the mean intensity for that neuron type), CALB+ matrix projection neurons showed the least intense GluR1, but the most intense GluR2 signal (Table 4). By contrast, the PARV+ perikarya showed the most intense GluR1 immunolabeling, and the GluR2 intensity in those PARV+ interneurons containing GluR2 was as high as in the CALB+ perikarya (Table 4). For ChAT+ and CALR+ interneuron perikarya, both GluR1 and GluR2 intensities were moderate, while for the SS+ interneurons GluR2 was much more intense than was GluR1. The relative rank order for the measured intensity of GluR1 immunostaining for those striatal neuron perikarya that were GluR1+, as assessed statistically, was PARV > CALR > ChAT > CALB = SS, while for those striatal neuron perikarya that were GluR2+, the measured GluR2 intensity rank order was CALB = PARV = SS > CALR = ChAT (Table 4). If one, however, includes perikarya lacking GluR1 or GluR2 in the calculation of mean intensity for GluR1 or GluR2 (respectively) for each neuron type (that is, calculate the mean intensity for all neurons of that type and not just those that were labeled for the given GluR), the rank order is slightly different, as shown in Table 4. Notably, CALB projection neurons are even more conspicuously rich in GluR2 than is true for the average perikaryon of any of the interneuron types (Table 4), while PARV interneurons are more than twice as rich in GluR1 as the average perikaryon of any of the other four neuron types compared. Based on the data shown in Table 4 for all neurons of a given type, we infer the rank order for the perikaryal GluR1:GluR2 ratio for these five neuron types to be PARV > CALR > ChAT > CALB > SS. While the intensity values have not been calibrated to actual GluR protein levels, it is useful to note that the GluR1:GluR2 ratios for the PARV and CALR perikarya approach 2.0, while those for the CALB and SS neurons are below 0.25. Thus, GluR1 appears to dominate over GluR2 in PARV and CALR perikarya, and GluR2 over GluR1 in CALB and SS neurons.

Comparisons among Striatal Projection Neuron Types—Among the striatal projection neurons distinguished by RDA3k labeling, perikarya retrogradely labeled from GPi showed the most intense GluR2 immunostaining and the least intense GluR1 immunostaining. Conversely, striatal perikarya retrogradely labeled from GPe had the lowest GluR2 immunostaining intensity, and the highest GluR1 immunostaining intensity (Table 5). The

relative intensity of GluR1 immunostaining for those striatal projection neurons that were GluR1+, as assessed statistically, was striato-GPe = striatonigral > striato-GPi, while for those striatal projection neurons that were GluR2+, it was striato-GPi >striatonigral = striato-GPe (Table 5). When perikarya lacking GluR1 are included in the calculation of mean GluR1 intensity for the neurons retrogradely labeled from a given striatal projection target (that is, calculate the mean intensity for all neurons of that type and not just for those that were labeled for GluR1), the rank order is slightly different (Table 5): striato-GPe > striatonigral > striato-GPi. Based on the data shown in Table 5 for all neurons RDA3k-labeled from a given striatal projection target, we infer the rank order for the perikaryal GluR1:GluR2 ratio for these three projection neuron types to be striato-GPe > striatonigral > striato-GPi. As in the case for CALB + perikarya, GluR2 appears to exceed GluR1 in the perikarya of all three projection neuron types, as the GluR1:GluR2 ratio is less than 0.5 in all three cases.

Note that since about 25% of striatal neurons retrogradely labeled from GPe are striato-GPi/nigral neurons labeled via their slight intra-GPe collateral, and since GluR1 intensity is relatively low among striato-GPi/nigral neurons, it seems likely that GluR1 intensity for striato-GPe type neurons per se is higher than the value shown for all neurons labeled from GPe. Similarly, striatal neurons labeled from GPi include some striatonigral type neurons labeled via their axon passing through GPi, and striatal neurons labeled from the nigra include some striato-GPi type neurons labeled via their collateral to the nigra. Thus, the GluR1 intensity for true striato-GPi neurons may be lower than the value shown for neurons labeled from GPi, and the GluR1 intensity for true striatonigral neurons may be higher than the value shown for neurons labeled from the nigra.

Patch versus Matrix—In the patch versus matrix comparison, the GluR1 immunostaining intensity of patch compartment perikarya was significantly greater than for matrix perikarya (Fig. 10), for both markers of compartmental identity (Table 6). By contrast, the perikaryal GluR2 intensity of medium-sized striosomal neurons did not differ significantly from that of matrix perikarya, using either the MOR or CALB markers to define compartmental identity (Fig. 10). Thus, striosomal projection neurons possess a higher GluR1:GluR2 ratio than do matrix projection neurons. In both cases, however, the ratio is well below 1.0, and so GluR2 appears to predominate even in striosomal perikarya.

Ultrastructural Localization of GluR1, GluR2 and GluR2/3 in Striatum

At the ultrastructural level, dark flocculent DAB reaction product for GluR1, GluR2/3 and GluR2 was found in the striatum in numerous dendritic spines and dendritic shafts (Fig. 11). Within the immunolabeled spines and dendrites, the reaction product was present in the cytoplasm, along the inner surfaces of cell membranes, around microtubules, or on the outer surfaces of mitochondria. Counts revealed that immunohistochemical labeling for GluR1 was present in about half of all striatal dendrites and nearly two-thirds of dendritic spines (Fig. 11A, B; Table 7). For GluR2/3, two-thirds of both dendrites and dendritic spines were immunostained (Fig. 11C, D; Table 7). For GluR2, about 40% of both dendrites and dendritic spines were immunolabeled (Fig. 11E, F; Table 7). As described previously (Bernard et al., 1997;Chen et al., 1998), the heads of many GluR-immunolabeled as well as many nonimmunolabeled spines received asymmetric synaptic contact from unlabeled axon terminals containing round vesicles clustered near the synaptic specialization. This was true of GluR-immunolabeled and nonimmunolabeled dendrites as well. The postsynaptic densities and the adjacent cytoplasm were prominently labeled for GluR1 (Fig. 11A,B), GluR2/3 (Fig. 11C, D) or GluR2 (Fig. 11E, F) in the immunolabeled spines and dendrites receiving such synaptic contacts. Since the dendritic spines in striatum belong to spiny projection neurons (Gerfen and Wilson, 1996) and since different types of striatal projection neurons differ in the size of the excitatory terminals their spines receive (Lei et al., 2004), we measured the size of

the asymmetric terminals making synaptic contact with spines heads, in an effort to characterize the types of striatal projection neurons possessing GluR1+, GluR2/3+ and GluR2+ spines. We found that asymmetric terminals synapsing on GluR1-immunolabeled spines were generally larger in diameter (0.614μm) than those on GluR2/3-immunolabeled spines (0.438μm) and than those on GluR2-immunolabeled spines (0.417μm). Terminals synapsing asymmetrically on GluR1-immunolabeled dendrites also tended to be larger (0.642μm) than those synaptically contacting GluR2/3-(0.455μm) or GluR2-immunostained dendrites (0.423μm) (Table 7). Since asymmetric axospinous terminals synapsing on striato-GPe neurons have been shown to average 0.6-0.7μm in diameter and those synapsing on striato-GPi/SN neurons have been shown to average 0.4-0.5μm in diameter (Lei et al., 2004), our present findings suggest that GluR1 is more common in the spines of striato-GPe neurons, and GluR2 and/or GluR3 more common in the spines of striato-GPi/SN neurons.

Discussion

We have shown that striatal neuron types differ in their relative content of GluR1 versus GluR2. Since R/G editing is about 80-90% complete in adult rat brain (Lomeli et al., 1994), R/G editing failure is unlikely to be a significant source of AMPA subunit variation among striatal neuron types. Similarly, RNA editing at the Q/R site of GluR2 is extremely efficient in postnatal rat brain, with only 1% of GluR2 subunits unedited (Carlson et al., 2000;Hollmann and Heinemann, 1994). Thus, in considering AMPA receptor function in the following sections, we will assume R/G and Q/R editing is complete, unless the evidence indicates otherwise for a given striatal neuron type.

Implications for AMPA Receptor Subunit Composition and Function of Striatal Neurons

Projection Neurons—*In situ* hybridization studies suggest striatal projection neurons in rats are richer in GluR2 than in GluR1, GluR3 or GluR4 mRNA (Catania et al., 1995). Consistent with this, single-cell RT-PCR studies have reported that all striatal projection neurons express GluR2, most express GluR1, but few express significant levels of GluR3, and none express GluR4 (Chen et al., 1998;Stefani et al., 1998;Vorobjev et al., 2000). A ubiquity of GluR2 in striatal projection neurons is consistent with previous immunohistochemical studies using polyclonal antibodies that recognize GluR2/3 or GluR2/3/4c (Tallaksen-Greene and Albin, 1994;Chen et al., 1996;Bernard et al., 1997). The monoclonal anti-GluR2 antibody used here (Vissavajjhala et al., 1996) confirmed that all striatal projection neuron perikarya contain GluR2 protein. Moreover, we found that striato-GPe and striatonigral neuron perikarya appear to contain less amounts of GluR2 than do striato-GPi neuron perikarya. The present study further shows that projection neuron perikarya are less rich in GluR1 than GluR2 protein, as also implied by prior ISHH, RT-PCR and immunolabeling studies, and that only 50-70% of striatal projection neuron perikarya contain GluR1 (Bernard et al., 1996,1997;Chen et al., 1996,1998;Stefani et al., 1998;Vorobjev et al., 2000). In contrast to the situation for GluR2, we found that striato-GPe perikarya are richer than striato-GPi perikarya in GluR1. Thus, at the level of perikaryal protein, striato-GPe neurons appear to have a higher GluR1:GluR2 ratio than do striato-GPi neurons, with striatonigral neurons intermediate. One consequence of this would be a tendency of striato-GPe and striatonigral neuron perikarya to have more AMPA receptors without GluR2 in their composition than do striato-GPi perikarya. Moreover, striato-GPi and striatonigral neurons are reported to have a lower flip:flop ratio than striato-GPe neurons (Tallaksen-Greene and Albin et al., 1996;Vorobjev et al., 2000).

Our data suggest that the differences in the GluR1:GluR2 ratio for striato-GPe versus striato-GPi/SNr neuron perikarya extend to the level of dendritic spines. This conclusion can be inferred from the greater mean size of the asymmetric axospinous terminals synapsing on GluR1+ than on GluR2+ (or GluR2/3+) spines, by the following reasoning. The mean size of

asymmetric axospinous terminals on striato-GPe neurons in rats is about 0.65μm while that on striato-GPi/SN neurons is about 0.44μm, reflecting a differential cortical input to these two types of striatal projection neurons (Lei et al., 2004). Striato-GPe neurons receive their main cortical input from pyramidal tract (PT) type cortical neurons of deep layer 5, which arises as a collateral of the descending PT projection to the ipsilateral brainstem and spinal cord (Wilson, 1987;Cowan and Wilson, 1994;Reiner et al., 2003). The intrastriatal axospinous PT-type terminals are relatively large (0.8μm) and their preferential input to striato-GPe neurons accounts for the relatively large mean size of asymmetric axospinous contacts on this neuron type. Striato-GPi/SNr neurons, by contrast, preferentially receive their cortical input from intratelencephalically projecting (IT-type) neurons of layer 3 and upper layer 5 that project bilaterally to striatum (Wilson, 1987;Cowan and Wilson, 1994;Reiner et al., 2003). The IT-type axospinous terminals are relatively small (0.4μm) and their preferential input to striato-GPi/SNr neurons accounts for the relatively small mean size of asymmetric axospinous contacts on this neuron type. Our present observation that asymmetric synaptic terminal size on GluR1 spines is about 0.61μm indicates that GluR1 spines must include many striato-GPe spines, and many striato-GPi/SNr spines as well. By contrast, our finding that asymmetric synaptic terminal size on GluR2 spines is 0.42μm suggests that the GluR2 spines we observed must be mainly striato-GPi/SNr spines. Thus, striato-GPi/SNr neuron spines possess both GluR1 and GluR2, while GluR1 predominates on striato-GPe spines. Since the size of asymmetric synaptic terminals on dendrites is similar to that on spines, it seems likely that striato-GPi/SNr neuron dendrites are enriched in both GluR1 and GluR2, and striato-GPe neuron dendrites in mainly GluR1.

Similar results were obtained for asymmetric synaptic terminal size on GluR2+ as for GluR2/3 + spines and dendrites. Given the scarcity of GluR3 in striatum, GluR2/3 localization in striatum should mainly reflect GluR2 localization. Nonetheless, 66% of striatal spines and dendrites immunolabeled for GluR2/3 (Bernard et al., 1997), but only 40% immunolabeled for GluR2. On the other hand, 100% of striatal projection neuron perikarya contained immunodetectable GluR2 protein in our LM studies. There are two possible explanations as to why both dendritic and spine localization of GluR2 and GluR2/3 are less than expected from their perikaryal localization. First, the glutaraldehyde fixation needed for EM tissue processing may diminish the sensitivity of GluR2 immunodetection. The difference between anti-GluR2/3 and anti-GluR2 in the frequency of spine and dendrite labeling may reflect a greater sensitivity of the anti-GluR2/3. Secondly, some spines may show use- or plasticity-dependent downregulation of GluR2 (Song and Huganir, 2002;Kolleker et al., 2003;Terashima et al., 2004). By contrast, the frequency of spines immunolabeled for GluR1 is more in agreement with the frequency of GluR1 in striatal perikarya, and with prior reports on GluR1 frequency in striatal spines (Bernard et al., 1997;Chen et al., 1998).

Since striatal patch neurons receive input from different cortical neurons than do matrix neurons, and project to a different part of the nigra than matrix striatonigral neurons (Wilson, 1990;Gerfen, 1992;Kincaid and Wilson 1996), it might be expected that patch neurons also differ in some ways from matrix neurons in AMPA subunit localization. We observed striosomal projection neurons (which project to the pars compacta) to be richer in GluR1 than matrix projection neurons (Martin et al., 1993a), but observed no such difference for GluR2. Thus, our results indicate that striato-SNc neurons have a higher GluR1: GluR2 ratio than any of the matrix striatal projection types.

Electrophysiological studies have confirmed that excitatory cortical input to striatal projection neurons is mediated by AMPA receptors (Kita, 1996;Calabresi et al., 1998), indicating that all projection neurons possess AMPA receptor in their dendrites and/or spines. While GluR2 subunits may predominate in striatal projection neurons, many projection neuron spines possess sufficient GluR2-lacking AMPA receptors to show AMPA receptor-mediated Ca^{2+}

influx (Carter and Sabatini, 2004). Since our data suggest that the spines of striato-GPe neurons are likely to possess more GluR2-lacking AMPA receptors than do striato-GPi neurons, striato-GPe spines may show greater Ca^{2+} influx via AMPA receptors than striato-GPi neurons, as well as desensitize more rapidly in response to cortical activation. Additionally, GluR2-lacking AMPA receptors show larger single-channel currents than do GluR2-possessing AMPA receptors (Swanson et al., 1997). The enhancement in AMPA-mediated Ca2+ entry, the faster desensitization, and the higher single-channel current associated with GluR2-lacking AMPA receptors, together with the preferential input from the large terminals of the PT-type corticostriatal neurons, and the perforated postsynaptic densities commonly associated with intrastriatal PT-type axospinous endings all may reflect or contribute to a role of striato-GPe neurons in the corticostriatal plasticity involved in movement refinement during procedural learning (Reiner et al., 2003;Lei et al., 2004;Plant et al., 2006). A preferential role of striato-GPe neurons and the ipsilateral PT-type input in corticostriatal plasticity is consistent with the finding that LTP is readily elicited in striatum by ipsilateral cortical stimulation but not by contralateral (IT-only) cortical stimulation (Wright et al., 2001). Differences in interactions with postsynaptic density proteins or in phosphorylation state between GluR1 and GluR2 might also promote synaptic plasticity in striato-GPe neurons (Song and Huganir, 2002;Kolleker et al., 2003;Terashima et al., 2004). By contrast, the AMPA receptor traits of striato-GPi neurons (and to a lesser degree striatonigral neurons) appear to favor the importance of a synchrony in the firing of cortical inputs for neuronal activation (input from smaller terminals, and receptors with smaller single-channel currents and slower desensitization), which might be related to their role in promoting behavior based on integration of inputs from diverse cortical areas (Albin et al., 1989;DeLong, 1990;Cowan and Wilson, 1994;Reiner et al., 2003;Lei et al., 2004).

Parvalbuminergic Interneurons—Previous studies reported that 50-70% of PARV+ neurons contain GluR2/3 or GluR2/3/4c-immunoreactivity (Tallaksen-Greene and Albin, 1994;Chen et al., 1996;Bernard et al., 1997). Our results show that 73% of PARV-containing neurons specifically contain GluR2. Two types of PARV+ striatal interneurons have been previously described (Kawaguchi, 1993), with one type (77% of all striatal PARV+ interneurons) having a local dendritic field, and the other an extended dendritic field. Given the similar frequency with which PARV+ neurons contain GluR2 and possess a localized dendritic tree, it is possible they are the same type. Prior immunocytochemical studies have shown intense immunolabeling for both GluR1 and GluR4 in all PARV+ striatal interneurons (Martin et al., 1993b;Tallaksen-Greene and Albin, 1994;Chen et al., 1996;Bernard et al., 1997;Kwok et al., 1997), and our current study confirmed this for GluR1.

Parvalbuminergic interneurons receive their major excitatory input from cerebral cortex, mainly as asymmetric axodendritic synaptic contacts (Kita et al., 1990,Kita, 1993), with the PARV+ interneurons forming symmetrical synaptic contacts on somata and dendrites of striatal projection neurons (Kita et al., 1990;Lapper et al., 1992). PARV+ interneurons fire phasically at high frequency in response to cortical stimulation (Kawaguchi, 1993;Kita, 1993). While the high spike rate of these neurons upon depolarization appears to reflect an intrinsic membrane property, their relative enrichment in cortical input and AMPA receptors accounts for their robust responses to cortical activation. Moreover, their specific enrichment in GluR1 and GluR4 compared to GluR2 (Martin et al., 1993b;Tallaksen-Greene and Albin, 1994;Chen et al., 1996;Bernard et al., 1997;Kwok et al., 1997) explains their inwardly rectifying I-V curve (Koos and Tepper, 1999), and indicates they are likely to mainly possess AMPA receptors with high calcium permeability, as typically true of PARV+ telencephalic neurons (Geiger et al., 1995;Götz et al., 1997;Kondo et al., 1997;Washburn et al., 1997). The higher single-channel conductance and faster desensitization of GluR1/4-rich AMPA receptors may also help explain the robust short duration action potentials in response to cortical activation (Kawaguchi, 1993;Koos and Tepper, 1999). The low levels of GluR2 in many PARV+ striatal interneurons

suggest that some neurons of this type may not show purely GluR1-GluR4 physiology, although the dendritic responses of this neuron type should be dominated by GluR2-lacking AMPA receptors.

Cholinergic Interneurons—ChAT+ striatal interneurons have not been reported to contain immunoreactivity for GluR2/3 or GluR2/3/4 in rats (Martin et al., 1993b;Tallaksen-Greene and Albin, 1994;Chen et al., 1996;Bernard et al., 1997;Kwok et al., 1997). Large aspiny interneurons that label for GluR2 by ISHH or immunohistochemistry have, however, been reported in human striatum (Bernard et al., 1996,Meng et al., 1997;Cicchetti et al., 1999). Additionally, single-cell RT-PCR studies on rat striatal neurons reported that 45-55% of large aspiny ChAT-containing neurons express GluR2 mRNA (Richardson et al., 2000;Vorobjev et al., 2000). Consistent with this, our present immunolabeling with a specific monoclonal antibody for GluR2 and the highly sensitive Alexa 488 fluorophore revealed that 55% of ChAT + neuronal perikarya in rat striatum contain GluR2 protein, albeit at relatively low levels. The current data also indicate that more than half of cholinergic striatal perikarya possess low levels of GluR1, and published data indicate at least 50% possess low levels of GluR3 and GluR4 (Bernard et al., 1996,1997;Vorobjev et al., 2000). The flop form of GluR1 and GluR4 appears to predominate (Vorobjev et al., 2000). Thus, more than half of striatal cholinergic neurons possess AMPA type glutamate receptors, and these may consist of GluR1-4 in relatively equal amounts. Cholinergic striatal interneurons receive limited excitatory input (Kawaguchi et al., 1995), predominantly from the thalamus (Lapper and Bolam, 1992). The finding that striatal cholinergic interneurons are poorer in AMPA receptors than are striatal projection neurons is consistent with the weak responses of striatal cholinergic neurons to cortical stimulation and AMPA receptor agonists (Bernard et al., 1996;Meng et al., 1997;Richardson et al., 2000;Vorobjev et al., 2000). The AMPA receptors of striatal cholinergic interneurons, however, have much higher Ca2+ permeability and faster desensitization times than those of projection neurons (Götz et al., 1997;Washburn et al., 1997;Vorobjev et al., 2000), which is consistent with the enrichment of cholinergic neurons in the flop forms of GluR1 and GluR4 relative to GluR2.

Somatostatinergic Interneurons—Striatal SS/NPY/NOS interneurons express only low levels of GluR1 and GluR2 (Catania et al., 1995;Kim et al., 2001), and the present results show that only about 50% contain detectable GluR2 protein and only 15% contain detectable GluR1 protein. Prior studies have also reported that few striatal NOS neurons contain GluR2 mRNA or protein, and even in these the levels are low (Catania et al., 1995;Bernard et al., 1997;Kim et al., 2001). The low GluR1 and GluR2 in this neuron type may explain why some prior studies failed to observe any GluR signal in it (Martin et al., 1993b,Tallaksen-Greene and Albin, 1994;Chen et al., 1996,Kwok et al., 1997). The paucity of GluR1 and GluR2 in SS/NPY/NOS interneurons is consistent with their minimal cortical glutamatergic input (Vuillet et al., 1989). Because NOS+ striatal neurons express the unedited form of GluR2 (Kim et al., 2001), the AMPA receptors that these neurons possess are likely to be Ca^{2+} permeable, and functionally significant in that AMPA increases striatal SS release (Hathway et al., 2001).

Calretinergic Interneurons—CALR+ striatal interneurons have medium-sized perikarya in rats (Bennett and Bolam, 1993;Kawaguchi et al., 1995;Figueredo-Cardenas et al., 1996b), but include both medium-sized and large aspiny neurons in human and primates (Fortin and Parent, 1994;Prensa et al., 1998). The medium-sized aspiny CALR+ striatal neurons in primate appear to correspond to the CALR+ interneurons found in rat striatum (Prensa et al., 1998), while the large CALR+ striatal neurons in primate also contain ChAT and thus correspond to the cholinergic striatal interneurons (Kawaguchi et al., 1995;Parent et al., 1995;Cicchetti et al., 2000). Cicchetti et al. (1999) reported GluR2 in about 80% of medium-sized CALR+ interneurons in human striatum, using the same antibody as in the present study. In contrast to

our findings indicating that only 33% of CALR+ perikarya in rat possess GluR2, with only low GluR2 levels even in these, Cicchetti et al. (1999) thus raise the possibility that GluR2 may be relatively more common in this neuron type in humans. We also found that 50% of CALR+ neuronal perikarya in rat striatum are rich in GluR1. Thus, in rats at least, CALR+ interneurons of striatum, in general, resemble PARV+ interneurons in having a high GluR1-GluR2 ratio. Similarly, Cicchetti et al. (1999) reported that about 40% of medium-sized CALR + neurons in human striatum possess GluR1, with 40% possessing GluR4 as well. While little is known of the physiology of this interneuron type, they are known to receive excitatory input that may be of cortical origin (Bennett and Bolam, 1993). Its apparently high GluR1-GluR2 ratio in rat suggests that its AMPA receptors are Ca^{2+} permeable, as is generally the case in brain for neurons containing either parvalbumin or calretinin (Kondo et al., 1997).

Implications for Vulnerability of Striatal Neurons

Role of AMPA receptors in striatal neuron degeneration—Numerous authors have hypothesized that the preferential death of striatal projection neurons and PARV+ interneurons that occurs in Huntington's disease and global ischemia is mediated by excitotoxicity (Beal. et al., 1986,1991;Chesselet et al., 1990;DiFiglia, 1990;Uemura, et al., 1990;Figueredo-Cardenas, et al., 1994,1997,1998;Ikonomidou and Turski, 1996;Paschen, 1996;Fusco et al., 1999;Meade et al., 2000), in particular by excess glutamate released from cortical terminals acting on striatal AMPA receptors (Schwarcz et al., 1984;Chen et al., 1999;Fusco et al., 1999;Popoli et al., 2002). Given the possible role of AMPA receptors in excitotoxic striatal injury (Chen et al., 1995), the question arises as to whether the differential localization of GluR1 and GluR2 contributes to differences in vulnerability among striatal neurons.

Projection Neurons versus Interneurons—The GluR2 subunit is related to excitotoxic vulnerability in two ways, as a reflection of AMPA receptor abundance and as a critical determinant of receptor physiology. Studies of mice overexpressing GluR2 indicate that excitotoxic vulnerability increases as the abundance of AMPA receptors increases (Le et al., 1997). For neurons possessing comparable AMPA receptor abundance, those expressing lower levels of GluR2 tend to be more vulnerable (Pellegrini-Giampietro et al., 1992,1997;Feldmeyer et al., 1999;Iihara et al., 2001). Such a phenomenon has been observed for CA1 pyramidal neurons, which downregulate their GluR2 levels after a transient ischemic episode (Pellegrini-Giampietro et al., 1997;Aronica et al., 1998). The resulting heightened Ca^{2+} entry is thought to initiate Ca^{2+}-mediated cellular injury, and be the means by which GluR2 insufficiency injures CA1 neurons (Blaschke et al., 1993;Tsubokawa et al., 1994). The excitotoxic vulnerability of spinal cord motoneurons is also thought to be mediated by GluR2-lacking AMPA receptors, and be attributable to either their Ca^{2+} permeability (Van Den Bosch et al., 2000), or their higher single channel conductance (Vandenberghe et al., 2000).

Striatal projection neurons receive extensive glutamatergic input and express abundant AMPA receptors, consistent with their preferential death in neurodegenerative disease and in excitotoxicity. The prominent cortical input to PARV+ interneurons, their low GluR2 levels in conjunction with their enrichment in GluR1 and GluR4, and their Ca^{2+}-permeable AMPA receptors are consistent with their high vulnerability to excitotoxic injury (Ferrer et al., 1994; Figuerado-Cardenas et al., 1998). The low GluR1-GluR4 levels characteristic of ChAT+, SS + and CALR+ interneurons and their sparse cortical input may explain their low vulnerability to excitotoxicity. Note that while CALB+ projection neurons, PARV+ interneurons, and CALR + interneurons are all defined by their enrichment in a particular calcium binding protein, possessing a calcium binding protein per se does not determine vulnerability in HD, since CALB+ projection neurons and PARV+ interneurons are vulnerable (Seto-Ohshima et al., 1988;Ferrer et al., 1994;Deng et al., 2004), and both the medium-sized CALR+ interneurons and the large cholinergic CALR+ interneurons are resistant (Cichetti et al., 1996, 2000).

Projection Neuron Differences—Striato-GPe and striatonigral neurons are more vulnerable in HD and ischemia than are striato-GPi neurons (Reiner et al., 1988;Albin et al., 1990a,b,1992;Richfield et al., 1995;Sapp et al., 1995;Meade et al., 2000;Deng et al., 2004). The higher GluR1: GluR2 ratio in striato-GPe neurons and the greater preponderance of flip subunits in striato-GPe neurons (Tallaksen-Greene and Albin et al., 1996;Vorobjev et al., 2000) implies they have greater Ca^{2+} influx and single-channel currents in response to excitatory stimulation, and are thus more likely to be damaged with overstimulation. In contrast, the lower GluR1: GluR2 ratio and the flop enrichment in striato-GPi neurons may make them less susceptible to the adverse effects of excitotoxic stimulation.

Patch versus matrix—Patch neurons appear more vulnerable than matrix neurons in the early stages of HD (Hedreen and Folstein, 1995) and to perinatal global ischemia (Burke and Baimbridge, 1993). We found that patch neurons have a higher GluR1: GluR2 ratio than do matrix neurons. Thus, the AMPA receptors of patch neurons may yield greater Ca^{2+} influx and higher single-channel currents, making them more vulnerable to overstimulation.

Summary

GluR1 is most common in parvalbuminergic interneurons, and GluR2 most common in projection neurons, with the rank order for the GluR1:GluR2 ratio being parvalbuminergic interneurons > calretinergic interneurons > cholinergic interneurons > projection neurons > somatostatinergic interneurons. The rank order for the GluR1:GluR2 ratio among striatal projection neurons was striato-GPe > striatonigral > striato-GPi. Striosomal projection neurons had a higher GluR1:GluR2 ratio than matrix projection neurons. The abundance of both GluR1 and GluR2 in striatal parvalbuminergic interneurons and projection neurons is consistent with their prominent cortical input and susceptibility to excitotoxic insult, while differences in GluR1:GluR2 ratio among projection neurons are likely to yield differences in Ca2+ permeability, desensitization, and single channel current, which may contribute to differences among them in plasticity, synaptic integration, and excitotoxic vulnerability.

Acknowledgements

We thank Drs. M.E.C. Fitzgerald, C. Meade, and A. Laverghetta for their useful comments and suggestions, and Kathy Troughten for technical assistance with EM. This research was supported by NS-19620 and NS 28721(A.R).

Abbreviations

AMPA, α-amino-3-hydroxy-5-methyl-ioxazole-4-propionic acid; CALB, calbindin; CALR, calretinin; ChAT, choline acetyltransferase; CLSM, confocal laser scanning microscope; EM, electron microscope; ENK, enkephalin; GPe, external segment, globus pallidus; GPi, internal segment, globus pallidus; HD, Huntington's disease; ISHH, in situ hybridization histochemistry; MOR, mu opiate receptor; NPY, neuropeptide Y; NHS, normal horse serum; NOS, nitric oxide synthase; PARV, parvalbumin; RDA3k, tetramethylrhodamine dextran amine, 3000MW; RT-PCR, reverse transcription-polymerase chain reaction; SN, substantia nigra; SNc, substantia nigra pars compacta; SNr, substantia nigra pars reticulata; SP, substance P; SS, somatostatin.

References

Albin RL, Reiner A, Anderson KD, Dure LS IV, Handelin B, Balfour R, Whetsell WO Jr. Penney JB, Young AB. Preferential loss of striato-external pallidal projection neurons in presymptomatic Huntington's disease. Ann. Neurol 1992;31:425–430. [PubMed: 1375014]

Albin RL, Reiner A, Anderson KD, Penney JB, Young AB. Striatal and nigral neuron subpopulations in rigid Huntington's disease: implications for the functional anatomy of chorea and rigidity-akinesia. Ann. Neurol 1990a;27:357–365. [PubMed: 1972318]

Albin RL, Young AB, Penney JB. The functional anatomy of basal ganglia disorders. Trends Neurosci 1989;12:366–375. [PubMed: 2479133]

Albin RL, Young AB, Penney JB, Handelin B, Balfour R, Anderson KD, Markel DS, Tourtellotte WW, Reiner A. Abnormalities of striatal projection neurons and N-Methyl-D-Aspartate receptors in presymptomatic Huntington's disease. N. Engl. J. Med 1990b;332:1923–1298.

Angulo MC, Lambolez B, Audinat E, Hestrin S, Rossier J. Subunit composition, kinetic, and permeation properties of AMPA receptors in single neocortical nonpyramidal cells. J. Neurosci 1997;17:6685–6696. [PubMed: 9254681]

Aoki C, Pickel VM. Neuropeptide Y in the cerebral cortex and caudate-putamen nuclei: ultrastructural basis for interactions with GABAergic and non-GABAergic neurons. J. Neurosci 1989;9:4333–4354. [PubMed: 2687439]

Aronica EM, Gorter JA, Grooms S, Kessler JA, Bennett MVL, Zukin RS, Rosenbaum DM. Aurintricarboxylic acid prevents GluR2 mRNA down-regulation and delayed neurodegeneration in hippocampal CA1 neurons of gerbil after global ischemia. Proc. Natl. Acad. Sci. USA 1998;95:7115–7120. [PubMed: 9618548]

Arvidsson U, Riedl M, Chakrabarti S, Lee JH, Nakano AH, Dado RJ, Loh HH, Law PY, Wessendorf MW, Elde R. Distribution and targeting of a mu-opioid receptor (MOR1) in brain and spinal cord. J. Neurosci 1995;15:3328–3341. [PubMed: 7751913]

Bazzett TJ, Becker JB, Katz KW, Albin RL. Chronic intrastriatal dialytic administration of quinolinc acid produces selective neural degeneration. Exp. Neurol 1993;120:177–185. [PubMed: 8387931]

Beal MF, Kowall NW, Ellison DW, Mazurek MF, Swartz KJ, Martin JB. Replication of the neurochemical characteristics of Huntington's disease by quinolinic acid. Nature 1986;321:168–171. [PubMed: 2422561]

Beal MF, Ferrante RJ, Swartz KJ, Kowall NW. Chronic quinolinic acid lesions in rats closely resemble Huntington's disease. J. Neurosci 1991;11:1649–1659. [PubMed: 1710657]

Bennett BD, Bolam JP. Characterization of calretinin-immunoreactive structures in the striatum of the rat. Brain Res 1993;609:137–148. [PubMed: 8508297]

Bennett BD, Callaway JC, Wilson CJ. Intrinsic membrane properties underlying spontaneous tonic firing in neostriatal cholinergic interneurons. J. Neurosci 2000;20:8493–8503. [PubMed: 11069957]

Bernard V, Gardiol A, Faucheux B, Bloch B, Agid Y, Hirsch EC. Expression of Glutamate receptors in the human and rat basal ganglia: effect of the dopaminergic denervation on AMPA receptor gene expression in the striatopallidal complex in Parkinson's disease and rat with 6-OHDA lesion. J. Comp. Neurol 1996;368:553–568. [PubMed: 8744443]

Bernard V, Somogyi P, Bolam JP. Cellular, subcellular, and subsynaptic distribution of AMPA-type glutamate receptor subunits in the neostriatum of the rat. J. Neurosci 1997;17:819–833. [PubMed: 8987803]

Blaschke M, Keller BU, Rivosecchi R, Hollmann M, Heinemann S, Konnerth A. A single amino acid determines the subunit-specific spider toxin block of alpha-amino-3-hydroxy-5-methylisoxazole-4-propionate/kainate receptor channels. Proc. Natl. Acad. Sci. U.S.A 1993;90:6528–6532. [PubMed: 8393569]

Bruce G, Wainer BH, Hersh LB. Immunoaffinity purification of human choline acetyltransferase: comparison of the brain and placental enzymes. J. Neurochem 1985;45:611–620. [PubMed: 4009177]

Burke RE, Baimbridge KG. Relative loss of the striatal striosome compartment, defined by calbindin-D28k immunostaining, following developmental hypoxic-ischemic injury. Neuroscience 1993;56:305–315. [PubMed: 8247262]

Burnashev N, Monyer H, Seeburg PH, Sakmann B. Divalent ion permeability of AMPA receptor channels is dominated by the edited form of a single subunit. Neuron 1992;8:189–198. [PubMed: 1370372]

Calabresi P, Centonze D, Pisani A, Sancesario G, Gubellini P, Marfia GA, Bernardi G. Striatal spiny neurons and cholinergic interneurons express differential ionotropic glutamatergic responses and vulnerability: Implications for ischemia and Huntington's disease. Ann. Neurol 1998;43:586–597. [PubMed: 9585352]

Carlson NG, Howard J, Gahring LC, Roger SW. RNA editing (Q/R site) and flop/flip splicing of AMPA receptor transcripts in young and old brains. Neurobiol Aging 2000;21:599–606. [PubMed: 10924778]

Carter AG, Sabatini BL. State-dependent calcium signaling in dendritic spines of striatal medium spiny neurons. Neuron 2004;44:483–493. [PubMed: 15504328]

Catania MV, Tolle TR, Monyer H, Differential expression of AMPA receptor subunits in NOS-positive neurons of cortex, striatum, and hippocampus. J. Neurosci 1995;15:7046–7061. [PubMed: 7472460]

Celio MR. Calbindin D-28k and parvalbumin in the rat nervous system. Neuroscience 1990;35:375–475. [PubMed: 2199841]

Celio MR, Baier W, Scharer L, de Viragh PA, Gerday C. Monoclonal antibodies directed against the calcium binding protein parvalbumin. Cell Calcium 1988;9:81–86. [PubMed: 3383226]

Celio MR, Baier W, Scharer L, Gregersen HJ, de Viragh PA, Norman AW. Monoclonal antibodies directed against the calcium binding protein Calbindin D-28k. Cell Calcium 1990;11:599–602. [PubMed: 2285928]

Chen Q, Harris C, Brown CS, Howe A, Sumeier DJ, Reiner A. Glutamate-mediated excitotoxic death of cultured striatal neurons is mediated by non-NMDA receptors. Exp. Neurol 1995;136:212–224. [PubMed: 7498411]

Chen Q, Veenman CL, Reiner A. Cellular expression of ionotropic glutamate receptor subunits on specific striatal neuron types and its implication for striatal vulnerability in glutamate receptor-mediated excitotoxicity. Neuroscience 1996;73:715–731. [PubMed: 8809793]

Chen Q, Veenman CL, Knopp K, Yan Z, Medina L, Song WJ, Surmeier DJ, Reiner A. Evidence for the preferential localization of GluR1 subunits of AMPA receptors to the dendritic spines of medium spiny neurons in rat striatum. Neuroscience 1998;83:749–761. [PubMed: 9483559]

Chen Q, Surmeier DJ, Reiner A. NMDA and non-NMDA receptor-mediated excitotoxicity are potentiated in cultured striatal neurons by prior chronic depolarization. Exp. Neurol 1999;159:283–296. [PubMed: 10486197]

Chesselet MF, Lin CS, Polsky K, Jin BK. Ischemic damage in the striatum of adults gerbils: relative sparing of somatostatinergic and cholinergic interneurons contrasts with loss of efferent neurons. Exp. Neurol 1990;110:209–218. [PubMed: 1977609]

Cicchetti F, Gould PV, Parent A. Sparing of striatal neurons coexpressing calretin and substance P (NK-1) receptor in Huntington's disease. Brain Res 1996;730:232–237. [PubMed: 8883909]

Cicchetti F, Parent A. Striatal interneurons in Huntington's disease: selective increase in the density of calretinin-immunoreactive medium sized neuron. Mov. Disord 1996;11:619–626. [PubMed: 8914086]

Cicchetti F, Prensa L, Wu Y, Parent A. Chemical anatomy of striatal interneurons in normal individuals and in patients with Huntington's disease. Brain Res. Rev 2000;34:80–101. [PubMed: 11086188]

Cicchetti F, Vinet J, Beach TG, Parent A. Differential expression of alpha-amino-3-hydroxy-5-methyl—4-isoxazolepropionate receptor subunits by calretinin immunoreactive neurons in the human striatum. Neuroscience 1999;93:89–97. [PubMed: 10430473]

Cowan RH, Wilson CJ. Spontaneous firing patterns and axonal projections of single corticostriatal neurons in the rat medial agranular cortex. J. Neurophysiol 1994;71:17–32. [PubMed: 8158226]

Dawbarn D, DeQuidt ME, Emson PC. Survival of basal ganglia neuropeptide Y-somatostatin neurons in Huntington's disease. Brain Res 1985;340:251–260. [PubMed: 2862959]

DeLong MR. Primate models of movement disorders of basal ganglia origin. Trends Neurosci 1990;13:281–285. [PubMed: 1695404]

Deng YP, Albin RL, Penney JB, Young AB, Anderson KD, Reiner A. Differential loss of striatal projection neurons in Huntington's disease: A quantitative immunohistochemical study. J. Chem. Neuroanat 2004;27:143–164. [PubMed: 15183201]

Deng YP, Lei WL, Reiner A. Differential perikayal localization in rats of D1 and D2 dopamine receptors on striatal projection neuron types identified by retrograde labeling. J. Chem. Neuroanat 2006;32:101–116. [PubMed: 16914290]

Desban M, Kemel ML, Glowinski J, Gauchy C. Spatial organization of patch and matrix compartments in the rat striatum. Neuroscience 1993;57:661–667. [PubMed: 8309529]

DiFiglia M. Excitotoxic injury of the striatum: a model for Huntington's disease. Trends Neurosci 1990;13:286–289. [PubMed: 1695405]

Feldmeyer D, Kask K, Brusa R, Kornau HC, Kolhekar R, Rozov A, Burnashev N, Jensen V, Hvalby O, Spremgel R, Seeburg PH. Neurological dysfunctions in mice expressing different levels of the Q/R site-edited AMPAR subunit GluR-B. Nat. Neurosci 1999;1:57–64. [PubMed: 10195181]

Ferrante RJ, Beal MF, Kowall NW, Richardson EP, Martin JB Jr. Sparing of acetylcholinesterase-containing striatal neurons in Huntington's disease. Brain Res 1987a;411:162–166. [PubMed: 2955849]

Ferrante RJ, Kowall NW, Beal MF, Martin JB, Bird ED, Richardson EP Jr. Morphological and histochemical characteristics of a spared subset of striatal neurons in Huntington's disease. J. Neuropathol. Exp. Neurol 1987b;46:12–27. [PubMed: 2947977]

Ferrante RJ, Kowall NW, Beal MF, Richardson EP, Bird ED, Martin JB. Selective sparing of a class of striatal neurons in Huntington's disease. Science 1985;230:561–563. [PubMed: 2931802]

Ferrer I, Kulisevsky J, Gonzalez G, Escartin A, Chivite A, Casas R. Parvalbumin-immunoreactive neurons in cerebral cortex and striatum in Huntington's disease. Neurodegeneration 1994;3:169–173.

Figueredo-Cardenas G, Anderson KD, Chen Q, Veenman CL, Reiner A. Relative survival of striatal projection neurons and interneurons after intrastriatal injection of quinolinic acid in rats. Exp. Neurol 1994;129:37–56. [PubMed: 7925841]

Figueredo-Cardenas G, Morello M, Sancesario G, Bernardi G, Reiner A. Colocalization of somatostatin, neuropeptide Y, neuronal nitric oxide synthase and NADPH-diaphorase in striatal interneurons in rats. Brain Res 1996a;735:317–324. [PubMed: 8911672]

Figueredo-Cardenas G, Medina L, Reiner A. Calretinin is localized to a unique population of striatal interneurons in rats. Brain Res 1996b;709:145–150. [PubMed: 8869567]

Figueredo-Cardenas G, Chen Q, Reiner A. Age-dependent differences in survival of striatal somatostatin-NPY-NADPH-diaphorase-containing interneurons versus striatal projection neurons after intrastriatal injection of quinolinic acid in rats. Exp. Neurol 1997;146:444–457. [PubMed: 9270055]

Figueredo-Cardenas G, Harris CL, Anderson KD, Reiner A. Relative resistance of striatal neurons containing calbindin or parvalbumin to quinolinic acid-mediated excitotoxicity compared to other striatal neuron types. Exp. Neurol 1998;149:356–372. [PubMed: 9500958]

Fortin M, Parent A. Patches in the striatum of squirrel monkeys are enriched with calretinin fibers but devoid of calretinin cell bodies. Neurosci. Lett 1994;182:51–54. [PubMed: 7891886]

Fusco FR, Chen Q, Lamoreaux WJ, Figueredo-Cardenas G, Jiao Y, Coffman JA, Surmeier DJ, Honig MG, Carlock LR, Reiner A. Cellular localization of huntingtin in striatal and cortical neurons in rats: lack of correlation with neuronal vulnerability in Huntington's disease. J. Neurosci 1999;19:1189–1202. [PubMed: 9952397]

Geiger JRP, Melcher T, Koh DS, Sakmann B, Seeburg PH, Jonas P, Monyer H. Relative abundance of subunit mRNA determines gating and ca2+ permeability of AMPA receptors in principal neurons and interneurons in the rat CNS. Neuron 1995;15:193–204. [PubMed: 7619522]

Gerfen CR. The neostriatal mosaic: multiple levels of compartmental organization in the basal ganglia. Ann. Rev. Neurosci 1992;15:285–320. [PubMed: 1575444]

Gerfen, CR.; Wilson, CJ. The basal ganglia. In: Swanson, LW.; Bjoklund, A.; Hokfelt, T., editors. Handbook of chemical neuroanatomy. 12. Elsevier; Amsterdam: 1996. p. 371-468.Integrated system of the CNS

Glass M, Dragunow M, Faull RLM. The pattern of neurodegeneration in Huntington's disease: a comparative study of cannobinoid, dopamine, adenosine and GABAa receptor alterations in the human basal ganglia in Hunting's disease. Neuroscience 2000;97:505–519. [PubMed: 10828533]

Götz T, Kraushaar U, Geiger J, Lubke J, Berger T, Jonas P. Functional properties of AMPA and NMDA receptors expressed in identified types of basal ganglia neurons. J. Neurosci 1997;17:204–215. [PubMed: 8987749]

Graybiel AM. Neurotransmitters and neuromodulators in the basal ganglia. Trends Neurosci 1990;13:244–254. [PubMed: 1695398]

Hathway GJ, Humphrey PP, Kendrick KM. Somatostatin release by glutamate in vivo is primarily regulated by AMPA receptors. Br. J. Pharmacol 2001;134:1155–1158. [PubMed: 11704634]

Hawker K, Lang AE. Hypoxic-ischemic damage of the basal ganglia: case reports and a review of the literature. Mov. Disord 1990;5:219–224. [PubMed: 2388637]

Hedreen JC, Folstein S. Early loss of neostriatal striosome neurons in Huntington's disease. J Neuropathol Exp. Neurol 1995;54:105–120. [PubMed: 7815073]

Hendry SH, Jones EG, DeFelipe J, Schmechel D, Brandon C, Emson PC. Neuropeptide-containing neurons of the cerebral cortex are also GABAergic. Proc. Natl. Acad. Sci. U.S.A 1984;81:6526–6530. [PubMed: 6149547]

Herlitze S, Raditsch M, Ruppersberg JP, Jahn W, Monyer H, Schoepfer R, Witzemann V. Argiotoxin detects molecular differences in AMPA receptor channels. Neuron 1993;10:1131–1140. [PubMed: 7686380]

Hollmann M, Heinemann S. Cloned glutamate receptors. Ann. Rev. Neurosci 1994;17:31–108. [PubMed: 8210177]

Hollmann M, Hartley M, Heinemann S. Ca2+ permeability of KA-AMPA-gated glutamate receptor channels depends on subunit composition. Science 1991;252:851–853. [PubMed: 1709304]

Iihara K, Joo DT, Henderson J, Sattlaer R, Taverna FA, Lourensen S, Orser BA, Rodeer JC, Tymianski M. The influence of glutamate receptor 2 expression on excitotoxicity in GluR2 null mutant mice. J. Neurosci 2001;21:2224–2239. [PubMed: 11264298]

Ikonomidou C, Turski L. Neurodegenerative disorders: clues from glutamate and energy metabolism. Crit. Rev. Neurobiol 1996;10:239–263. [PubMed: 8971131]

Jog MS, Kubota Y, Connolly CI, Hillegaart V, Graybiel AM. Building neural representations of habits. Science 1999;286:1745–1749. [PubMed: 10576743]

Jonas P, Burnashev N. Molecular mechanisms controlling calcium entry through AMPA-type glutamate receptor channels. Neuron 1995;15:987–990. [PubMed: 7576666]

Jonas P, Racca C, Sakmann B, Seeburg PH, Monyer H. Differences in Ca2+ permeability of APMA-type glutamate receptor channels in neocortical neurons caused by differential GluR-B subunit expression. Neuron 1994;12:1281–1289. [PubMed: 8011338]

Kagi U, Berchtold MW, Heizmann CW. Ca2+-binding parvalbumin in rat testis. Characterization, localization, and expression during development. J. Biol. Chem 1987;262:7314–7320. [PubMed: 3294830]

Kawaguchi Y, Wilson CJ, Emson PC. Projection subtypes of rat neostriatal matrix cells revealed by intracellular injection of biocytin. J. Neurosci 1990;10:3421–3238. [PubMed: 1698947]

Kawaguchi Y. Physiological, morphological, and histochemical characterization of three classes of interneurons in rat neostriatum. J. Neurosci 1993;13:4908–4923. [PubMed: 7693897]

Kawaguchi Y, Wilson CJ, Augood SJ, Emson PC. Striatal interneurons: chemical, physiological and morphological characterization. Trends Neurosci 1995;18:527–535. [PubMed: 8638293]

Keinanen K, Wisden W, Sommer B, Werner P, Herb A, Verdoorn TA, Sakamann B, Seeberg PH. A family of AMPA-selective glutamate receptors. Science 1990;249:556–560. [PubMed: 2166337]

Kim DY, Kim SH, Choi HB, Min C, Gwag BJ. High abundance of GluR1 mRNA and reduced Q/R editing of GluR2 mRNA in individual NADPH-diaphorase neurons. Mol. Cell Neurosci 2001;17:1025–1033. [PubMed: 11414791]

Kincaid AE, Wilson CJ. Corticostriatal innervation of the patch and matrix in the rat neostriatum. J. Comp. Neurol 1996;374:578–592. [PubMed: 8910736]

Kita H. GABAergic circuits of the striatum. Prog. Brain Res 1993;99:51–72. [PubMed: 8108557]

Kita H. Glutamatergic and GABAergic postsynaptic responses of striatal spiny neurons to intrastriatal and cortical stimulation recorded in slice preparations. Neuroscience 1996;70:925–940. [PubMed: 8848174]

Kita H, Kosaka T, Heizmann CW. Parvalbumin-immunoreactive neurons in the rat neostriatum: a light and electron microscopic study. Brain Res 1990;536:1–15. [PubMed: 2085740]

Kolleker A, Zhu JJ, Schupp BJ, Qin Y, Mack V, Borchardt T, Köhr G, Malinow R, Seeburg PH, Olsen P. Glutamatergic plasticity by synaptic delivery of GluR-B_{long}-containing AMPA receptors. Neuron 2003;40:1199–1212. [PubMed: 14687553]

Kondo M, Sumino R, Okado H. Combinations of AMPA subunit expression in individual cortical neurons correlate with expression of specific calcium-binding proteins. J. Neurosci 1997;17:1570–1581. [PubMed: 9030617]

Koos T, Tepper JM. Inhibitory control of neostriatal projection neurons by GABAergic interneurons. Nat. Neurosci 1999;2:467–472. [PubMed: 10321252]

Kowall NW, Ferrante RJ, Martin JB. Pattern of cell loss in Huntington's disease. Trends Neurosci 1987;10:24–29.

Kubota Y, Mikawa S, Kawaguchi Y. Neostriatal GABAergic interneurons contain NOS, calretinin or parvalbumin. NeuroReport 1993;5:205–208. [PubMed: 7507722]

Kwok KHH, Tse YC, Wong RNS, Yung KKL. Cellular localization of GluR1, GluR2/3 and GluR4 glutamate receptor subunits in neurons of the rat neostriatum. Brain Res 1997;778:43–55. [PubMed: 9462876]

Lapper SR, Bolam JP. Input from the frontal cortex and the parafascicular nucleus to cholinergic interneurons in the dorsal striatum of the rat. Neuroscience 1992;51:533–545. [PubMed: 1488113]

Lapper SR, Smith Y, Sadikot AF, Parent A, Bolam JP. Cortical input to parvalbumin-immunoreactive neurones in the putamen of the squirrel monkey. Brain Res 1992;580:215–224. [PubMed: 1504801]

Le D, Das S, Wang YF, Yoshizawa T, Sasaki YF, Takasu M, Nemes A, Mendelsohn M, Dikkes P, Lipton SA, Nakanishi N. Enhanced neuronal death from focal ischemia in AMPA-receptor transgenic mice. Mol. Brain Res 1997;52:235–241. [PubMed: 9495544]

Lei WL, Jiao Y, Del Mar N, Reiner A. Evidence for differential cortical input to direct pathway versus indirect pathway striatal projection neurons in rats. J. Neurosci 2004;24:8289–8299. [PubMed: 15385612]

Lomeli H, Mosbacher J, Melcher T, Hoger T, Geiger JR, Kuner T, Monyer H, Higuchi M, Bach A, Seeburg PH. Control of kinetic properties of AMPA receptor channels by nuclear RNA editing. Science 1994;266:1709–1713. [PubMed: 7992055]

Martin LJ, Blackstone CD, Huganir RL, Price DL. The striatal mosaic in primates: striasomes and matrix are differentially enriched in ionotropic glutamate receptor subunits. J. Neurosci 1993a;13:782–792. [PubMed: 7678861]

Martin LJ, Blackstone CD, Levey AI, Huganir RL, Price DL. AMPA glutamate receptor subunits are differentially distributed in rat brain. Neuroscience 1993b;53:327–358. [PubMed: 8388083]

Meade CA, Deng YP, Fusco FR, Del Mar N, Hersch S, Goldowitz D, Reiner A. Cellular localization and development of neuronal intranuclear inclusions in striatal and cortical neurons in R6/2 transgenic mice. J. Comp. Neurol 2002;449:241–269. [PubMed: 12115678]

Meade CA, Figueredo-Cardenas G, Fusco F, Nowak TS Jr. Pulsinelli WA, Reiner A. Transient global ischemia in rats yields striatal projection neuron and interneuron loss resembling that in Huntington's disease. Exp. Neurol 2000;166:307–323. [PubMed: 11085896]

Meng SZ, Obonai T, Isumi H, Takashima S. A developmental expression of AMPA-selective glutamate receptor subunits in human basal ganglia. Brain Development 1997;19:388–392. [PubMed: 9339865]

Ono M, Murakami T, Kudo A, Isshiki M, Sawada H, Segawa A. Quantitative comparison of anti-fading mounting media for confocal laser scanning microscopy. J. Histochem. Cytochem 2001;49:305–311. [PubMed: 11181733]

Panchuk-Voloshina N, Haugland RP, Bishop-Stewart J, Bhalgat MK, Millard PJ, Mao F, Leung WY, Haugland RP. Alexa dyes, a series of new fluorescent dyes that yield exceptionally bright, photostable conjugates. J. Histochem. Cytochem 1999;47:1179–1188. [PubMed: 10449539]

Parent A, Cicchetti F, Beach TG. Calretinin-immunoreactive neurons in the human striatum. Brain Res 1995;674:347–351. [PubMed: 7796115]

Paschen W. Glutamate excitotoxicity in transient global cerebral ischemia. Acta Neurobiol. Exp 1996;56:313–322.

Paxinos, G.; Watson, C. The rat brain in stereotaxic coordinates. Fourth Edition. Academic Press; New York: 1998.

Pellegrini-Giampietro DE, Gorter JA, Bennett MVL, Zukin RS. The GluR2(GluR-B) hypothesis:Ca2+-permeable AMPA receptors in neurological disorders. Trends Neurosci 1997;20:464–470. [PubMed: 9347614]

Pellegrini-Giampietro DE, Zukin RS, Bennett MV, Cho S, Pulsinelli WA. Switch in glutamate receptor subunit gene expression in CA1 subfield of hippocampus following global ischemia in rats. Proc. Natl. Acad. Sci. U.S.A 1992;89:10499–10503. [PubMed: 1438239]

Petralia RS, Wenthold RJ. Light and electron immunocytochemical localization of AMPA-selective glutamate receptors in the rat brain. J. Comp. Neurol 1992;318:329–354. [PubMed: 1374769]

Plant K, Pelkey KA, Bortolotto ZA, Morita D, Terashima A, McBain CJ, Collingridge GL, Isaac JTR. Transient incorporation of native GluR2-lacking AMPA receptors during hippocampal long-term potentiation. Nat. Neurosci 2006;9:602–604. [PubMed: 16582904]

Popoli P, Pintor A, Domenici MR, Frank CM, Rebano T, Pezzola A, Scarchilli L, Quarta D, Reggio R, Malchiodi-Albedi F, Falchi M, Massotti M. Blockade of striatal Adenosine A_{2A} receptor reduces, through a presynatpic mechanism, quinolinic acid-induced excitotoxicity: Possible relevance to neuroprotective interventions in neurodegenerative disease of the striatum. J. Neurosci 2002;22:1967–1975. [PubMed: 11880527]

Prensa L, Gimenez-Agaya JM, Parent A. Morphological features of neurons containing calcium binding proteins in the human striatum. J. Comp. Neurol 1998;390:552–563. [PubMed: 9450535]

Reiner A, Albin RL, Anderson KD, D'Amato CJ, Penney JB, Young AB. Differential loss of striatal projection neurons in Huntington's disease. Proc. Natl. Acad. Sci. U.S.A 1988;85:5733–5737. [PubMed: 2456581]

Reiner A, Anderson KD. The patterns of neurotransmitter and neuropeptide co-occurrence among striatal projection neurons: Conclusions based on recent findings. Brain Res. Rev 1990;15:251–265. [PubMed: 1981156]

Reiner A, Veenman CL, Medina L, Jiao Y, Del Mar N, Honig MG. Pathway tracing using biotinylated dextran amines. J. Neurosci. Methods 2000;103:23–37. [PubMed: 11074093]

Reiner A, Jiao Y, Del Mar N, Laverghetta AV, Lei WL. Differential morphology of pyramidal-tract type and intratelencephalically-projecting type corticostriatal neurons and their intrastriatal terminals in rats. J. Comp. Neurol 2003;457:420–440. [PubMed: 12561080]

Richardson PJ, Dixon AK, Lee K, Bell MI, Cox PJ, Williams R, Pinnock RD, Freeman TC. Correlating physiology with gene expression in striatal cholinergic neurones. J. Neurochem 2000;74:839–846. [PubMed: 10646537]

Richfield EK, Maguire-Zeiss KA, Cox C, Gilmore J, Voorn P. Reduced expression of preproenkephalin in striatal neurons from Huntington's disease patients. Ann. Neurol 1995;37:335–343. [PubMed: 7695232]

Rogers SW, Hughes TE, Hollmann M, Gasic GP, Deneris ES, Heinemann S. The characterization and localization of the glutamate receptor subunit GluR1 in the rat brain. J. Neurosci 1991;11:2713–2724. [PubMed: 1652625]

Sapp E, Ge P, Aizawa H, Bird E, Penney J, Young AB, von Sattel JP, DiFiglia M. Evidence for a preferential loss of enkephalin immunoreactivity in the external globus pallidus in low grade Huntington's disease using high resolution image analysis. Neuroscience 1995;64:397–404. [PubMed: 7535402]

Sato K, Kiyama H, Tohyama M. The differential expression patterns of messenger RNAs encoding non-N- methyl-D-aspartate glutamate receptor subunits (GluR1-4) in the rat brain. Neuroscience 1993;52:515–539. [PubMed: 8450957]

Schwarcz RAC, Foster ED, French WO, Whetsell, Kohler C. Excitoxic models for neurodegenerative disorders. Life Sci 1984;35:19–32. [PubMed: 6234446]

Schwaller B, Buchwald P, Blumcke I, Celio MR, Hunziker W. Characterization of a polyclonal antiserum against the purified human recombinant calcium binding protein calretinin. Cell Calcium 1993;14:639–48. [PubMed: 8242719]

Seidenman KJ, Steinberg JP, Huganir R, Malinow R. Glutamate receptor subunit 2 serine 880 phosphorylation modulates synaptic transmission and mediates plasticity in CA1 pyramidal cells. J. Neuroci 2003;23:9220–9228.

Seto-Ohshima A, Emson PC, Lawson E, Mountjoy CQ, Carrasco LH. Loss of matrix calcium-binding protein-containing neurons in Huntington's disease. Lancet 1988;1(8597):1252–1255. [PubMed: 2897519]

Shiromani PJ, Armstrong DM, Bruce G, Hersh LB, Groves PM, Gillin JC. Relation of pontine choline acetyltransferase immunoreactive neurons with cells which increase discharge during REM sleep. Brain Res. Bull 1987;18:447–455. [PubMed: 3580914]

Somogyi P, Bolam JP, Smith AD. Monosynaptic cortical input and local axon collaterals of identified striatonigral neurons. A light and electron microscopic study using the Golgi-peroxidase transport-degeneration procedure. J. Comp, Neurol 1981;195:567–584. [PubMed: 6161949]

Song I, Huganir R. Regulation of AMPA receptors during synaptic plasticity. Trends Neurosci 2002;25:578–588. [PubMed: 12392933]

Stefani A, Chen Q, Flores-Hernandez J, Jiao Y, Reiner A, Surmeier DJ. Physiological and molecular properties of AMPA/KA receptors expressed by striatal medium spiny neurons. Dev. Neurosci 1998;20:242–252. [PubMed: 9691198]

Svingos AL, Moriwaki A, Wang JB, Uhl GR, Pickel VM. Ultrastructural immunocytochemical localization of mu-opioid receptors in rat nucleus accumbens: extrasynaptic plasmalemmal distribution and association with Leu5-enkephalin. J. Neurosci 1996;16:4162–4173. [PubMed: 8753878]

Swanson GT, Kamboj SK, Cull-Candy SG. Single-channel properties of recombinant AMPA receptors depend on RNA editing, splice variation, and subunit composition. J. Neurosci 1997;17:58–69. [PubMed: 8987736]

Tallaksen-Greene SJ, Albin RL. Localization of AMPA-selective excitatory amino acid receptor subunits in identified populations of striatal neurons. Neuroscience 1994;61:509–519. [PubMed: 7969927]

Tallaksen-Greene SJ, Albin RL. Splice variants of glutamate receptor subunits 2 and 3 in striatal projection neurons. Neuroscience 1996;75:1057–1064. [PubMed: 8938741]

Terashima A, Cotton L, Dev KK, Meyer G, Zaman S, Duprat F, Henley JM, Collingridge GL, Isaac JTR. Regulation of synaptic strength and AMPA receptor subunit composition by PICK1. J. Neurosci 2004;24:5381–5390. [PubMed: 15190111]

Tsubokawa H, Oguro K, Masuzawa T, Kawai N. Ca(2+)-dependent non-NMDA receptor-mediated synaptic currents in ischemic CA1 hippocampal neurons. J. Neurophysiol 1994;71:1190–1196. [PubMed: 8201412]

Uemura Y, Kowall NW, Beal MF. Selective sparing of NADPH-diaphorase-somatostatin-neuropeptide Y neurons in ischemic gerbil striatum. Ann. Neurol 1990;27:620–625. [PubMed: 1972876]

Van Damme P, Van Den Bosch L, Van Houtte E, Callewaert G, Robberrecht W. GluR2-dependent properties of AMPA receptors determine the selective vulnerability of motor neurons to excitotoxicity. J. Neurophysiol 2002;88:1279–1287. [PubMed: 12205149]

Van Den Bosch L, Vandenberghe W, Klaassen H, Van Houtte E, Robberecht W. Ca2+-permeable AMPA receptors and selective vulnerability of motor neurons. J. Neurol. Sci 2000;180:29–34. [PubMed: 11090861]

Vandenberghe W, Robberecht W, Brorson JR. AMPA receptor calcium permeability, GluR2 expression, and selective motoneuron vulnerability. J. Neurosci 2000;20:123–132. [PubMed: 10627588]

Vincent SR, Johansson O. Striatal neurons containing both somatostatin- and avian pancreatic polypeptide (APP)-like immunoreactivities and NADPH-diaphorase activity: a light and electron microscopic study. J. Comp. Neurol 1983;217:264–270. [PubMed: 6136532]

Vissavajjhala P, Janssen WGM, Hu Y, Gazzaley AM, Moran T, Hof PR, Morrison JH. Synaptic distribution of the AMPA-GluR2 subunit and its colocalization with calcium-binding proteins in rat cerebral cortex: an immunohistochemical study using a GluR2-specific monoclonal antibody. Exp. Neurol 1996;142:296–312. [PubMed: 8934561]

Vonsattel J-P, DiFiglia M. Huntington disease. J. Neuropathol. Exp. Neurol 1998;57:369–384. [PubMed: 9596408]

Vonsattel J-P, Myers RH, Stevens TJ, Ferrante RJ, Bird ED, Richardson EP. Neuropathological classification of Huntington's disease. J. Neuropathol. Exp. Neurol 1985;44:559–577. [PubMed: 2932539]

Vorobjev VS, Sharonova IN, Haas HL, Sergeeva OA. Differential modulation of AMPA receptors by cyclothiazide in two types of striatal neurons. Eur. J. Neurosci 2000;12:2871–2880. [PubMed: 10971630]

Vuillet J, Kerkerian L, Kachidian P, Bosler O, Nieoullon A. Ultrastructural correlates of functional relationships between nigral dopaminergic or cortical afferent fibers and neuropeptide Y-containing neurons in the rat striatum. Neurosci. Lett 1989;100:99–104. [PubMed: 2761790]

Wang H, Pickel V. Dendritic spines containing μ-Opioid receptors in rat striatal patches receive asymmetric synapses from prefrontal corticostriatal afferents. J. Comp. Neurol 1998;396:223–237. [PubMed: 9634144]

Wang HB, Laverghetta AV, Foehring R, Deng YP, Sun Z, Yamamoto K, Lei WL, Jiao Y, Reiner A. Single-cell RT-PCR, in situ hybridization histochemistry, and immunohistochemical studies of substance P and enkephalin co-occurrence in striatal projection neurons in rats. J. Chem. Neuroanat 2006;31:178–199. [PubMed: 16513318]

Washburn MS, Numberger M, Zhang S, Dingledine R. Differential dependence on GluR2 expression of three characteristic features of AMPA receptors. J. Neurosci 1997;17:9393–9406. [PubMed: 9390995]

Wenthold RJ, Yokotani N, Doi K, Wada K. Immunochemical characterization of the non-NMDA glutamate receptor using subunit-specific antibodies. Evidence for a hetero-oligomeric structure in rat brain. J. Biol. Chem 1992;267:501–507. [PubMed: 1309749]

Wilson CJ. Morphology and synaptic connections of crossed corticostriatal neurons in the rat. J. Comp. Neurol 1987;263:567–580. [PubMed: 2822779]

Wilson, CJ. Basal Ganglia. In: Shepard, GM., editor. The synaptic organization of the brain. Oxford University Press; New York: 1990. p. 279-316.

Wilson, CJ. Dendritic morphology, inward rectification and the functional properties of neostriatal neurons. In: McKenna, T.; Davis, J.; Kornetzer, SF., editors. Single Neuron Computation. Academic Press; San Diego: 1992. p. 141-171.

Wilson, CJ. The contribution of cortical neurons to the firing pattern of striatal spiny neurons. In: Houk, JC.; Davis, JL.; Beiser, DG., editors. Models of Information Processing in the Basal Ganglia. MIT Press; Cambridge, Massachusetts: 1995. p. 29-50.

Wright AK, Ramanathan S, Arbuthnott GW. Identification of the source of the bilateral projection system from cortex to somatosensory neostriatum and an exploration of its physiological actions. Neuroscience 2001;103:87–96. [PubMed: 11311789]

Wu Y, Richard S, Parent A. The organization of the striatal output system: a single-cell juxtacellular labeling study in the rat. Neuroscience Res 2000;38:49–62.

Zimmermann L, Schwaller B. Monoclonal antibodies recognizing epitopes of calretinins: dependence on Ca2+-binding status and differences in antigen accessibility in colon cancer cells. Cell Calcium 2002;31:13–25. [PubMed: 11990296]

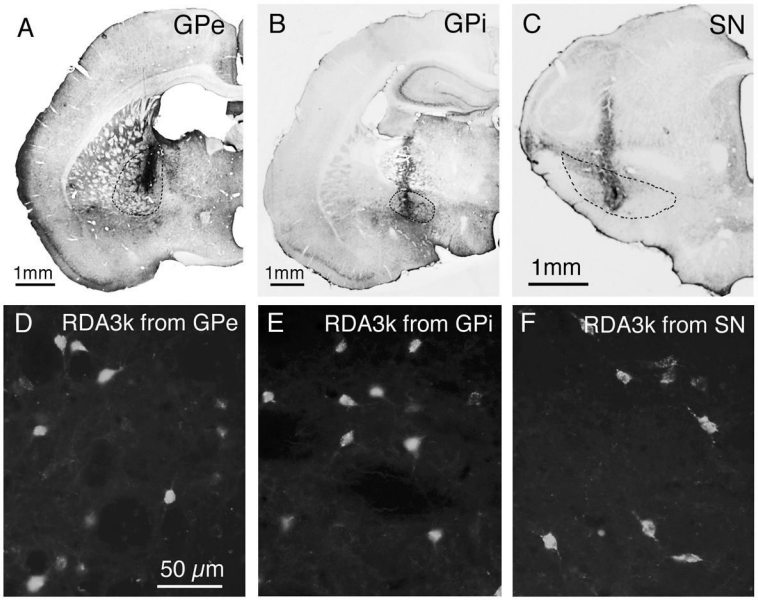

Fig 1.

Examples of RDA3k injection sites in the external part of globus pallidus (A), internal part of globus pallidus (B) or substantia nigra (C) at low magnification, and of retrogradely labeled neurons in striatum from those injections at high magnification (D–F; respectively). The injection sites in A–C have been visualized using peroxidase-antiperoxidase immunolabeling with DAB as the chromogen, using an antiserum against rhodamine to detect the RDA3k, and the intended injection target is delineated with dashed lines. The RDA3k-labeled striatal neurons in D-F have been visualized using epi-illumination fluorescence microscopy. Magnification in D–F is the same. For abbreviations, see list.

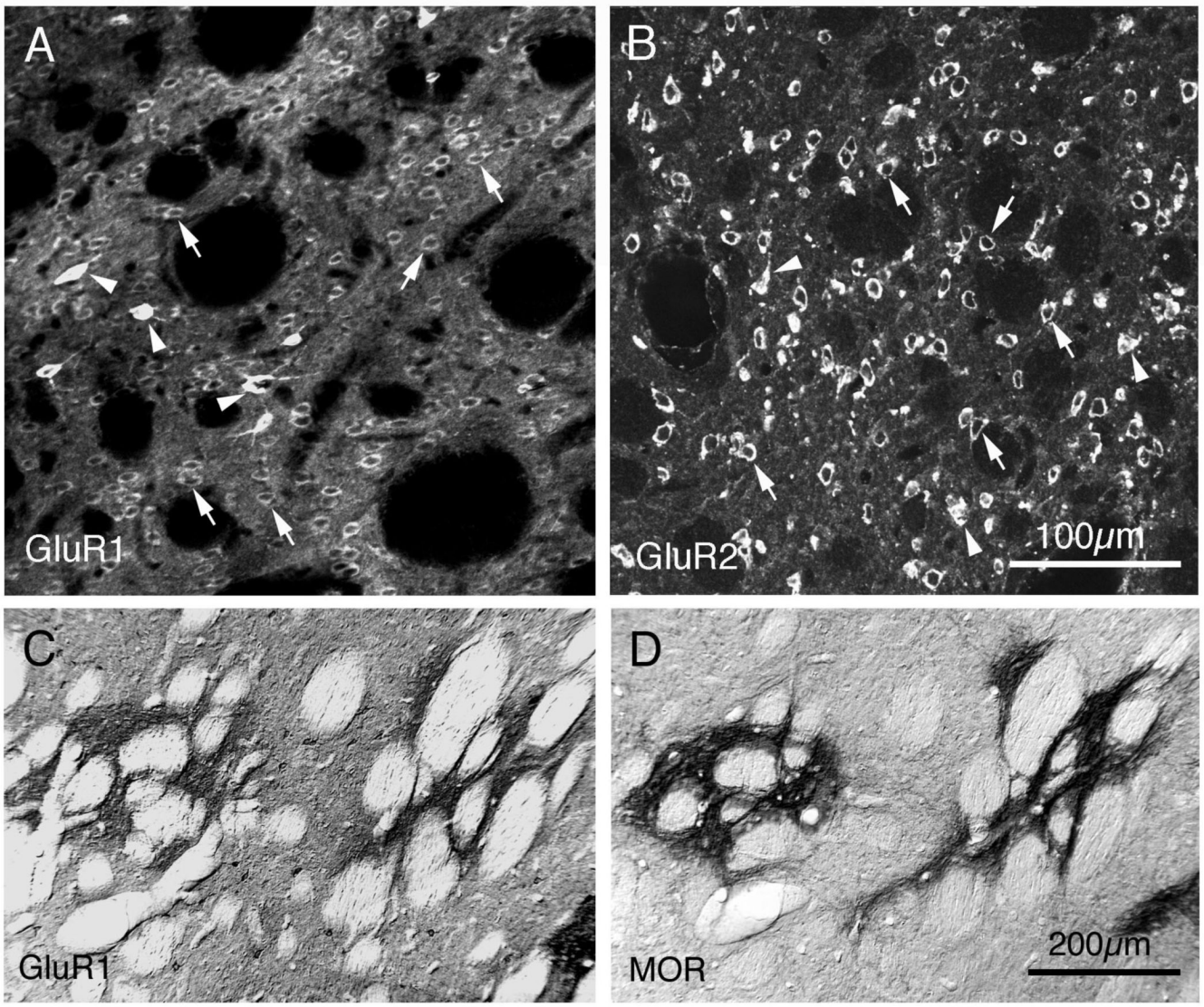

Fig 2.

Images of GluR1 and GluR2 immunolabeling in rat striatum. Panels A and B show CLSM images of sections through rat striatum that had been single-labeled for GluR1 (A) or GluR2 (B) using immunofluorescence with Alexa 488 as the fluorophore. Image A shows that GluR1-immunostaining was ample, with both neuropil and perikarya labeled. The GluR1+ perikarya included numerous moderately labeled, medium-sized ones (likely to belong to projection neurons, and indicated by arrows), intensely immunolabeled medium to large-sized ones (indicated by arrowheads, and likely to belong to parvalbuminergic neurons), and yet more rare large, moderately labeled ones (likely to belong to cholinergic neurons). Image B shows that GluR2-immunoreactive perikarya were more distinct than the GluR1-immunoreactive perikarya, due to the low level of background and neuropil labeling and the intensity of the GluR2 immunolabeling. The GluR2+ perikarya were highly abundant and widespread in striatum and included both medium-sized (arrows) and large perikarya (arrowheads), all similar in their labeling intensity. These images each represent ten collapsed 1μm interval CLSM images. Scale bar = 100μm in both A and B. Images C and D show the concordance between the GluR1-enriched striatal patches (C) and the striosomal compartment, as defined by MOR

immunolabeling (D). Panels C and D are from adjacent rat brain sections that had been immunolabeled by the peroxidase-antiperoxidase method using DAB. Magnification in A is the same as in B, and in C is the same as in D. For abbreviations, see list.

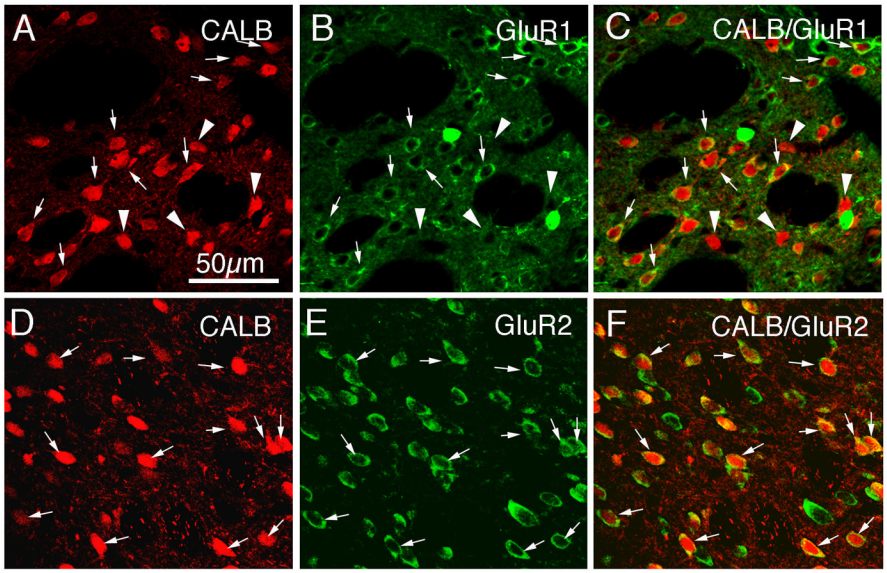

Fig 3.

CLSM images of GluR1 (A–C) and GluR2 (D–F) immunolabeling in calbindinergic (CALB +) striatal matrix projection neuron perikarya in rat. The GluR1 (B) or GluR2 (E) immunolabeling was visualized with Alexa 488 (green), while the CALB+ (A, D) immunolabeling was visualized with Alexa 594 (red). Perikaryal double-labeling is evident as a yellow-orange ring (C, F), reflecting an overlap of the green cytoplasmic labeling for GluR1 or GluR2 with the red cytoplasmic labeling for CALB. In the images shown, CALB+ perikarya containing GluR1 or GluR2 are indicated by arrows, while CALB+ perikarya lacking GluR1 are indicated by arrowheads. Only a little more than half of the CALB+ perikarya immunolabeled for GluR1, while all CALB+ neurons immunolabeled for GluR2. Magnification is the same in all images. For abbreviations, see list.

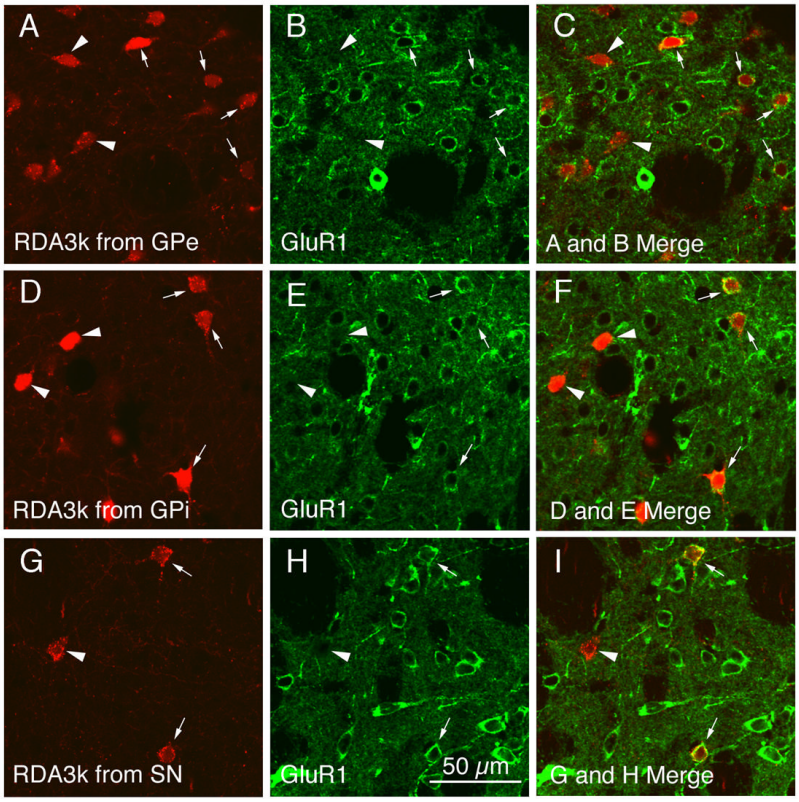

Fig 4.

CLSM images of GluR1 immunofluorescence in neuronal perikarya that had been retrogradely RDA3k-labeled from GPe (A–C), GPi (D–F), or SN (G–I). The GluR1 immunolabeling (B, E, H) was visualized with Alexa 488 (green), while the neuronal perikarya retrogradely labeled from GPe (A), GPi (D), or SN (G) were labeled with RDA3k (red). Perikaryal double-labeling is evident as a yellow-orange ring (C, F, I), reflecting an overlap of the green cytoplasmic labeling for GluR1 with the red RDA3k in the retrogradely labeled perikarya. Double-labeled perikarya are indicated by arrows, while RDA3k-labeled perikarya lacking GluR1 are indicated by arrowheads. Note that not all striatal perikarya retrogradely labeled from GPe, GPi, or SN immunolabeled for GluR1. Magnification is the same in all images. For abbreviations, see list.

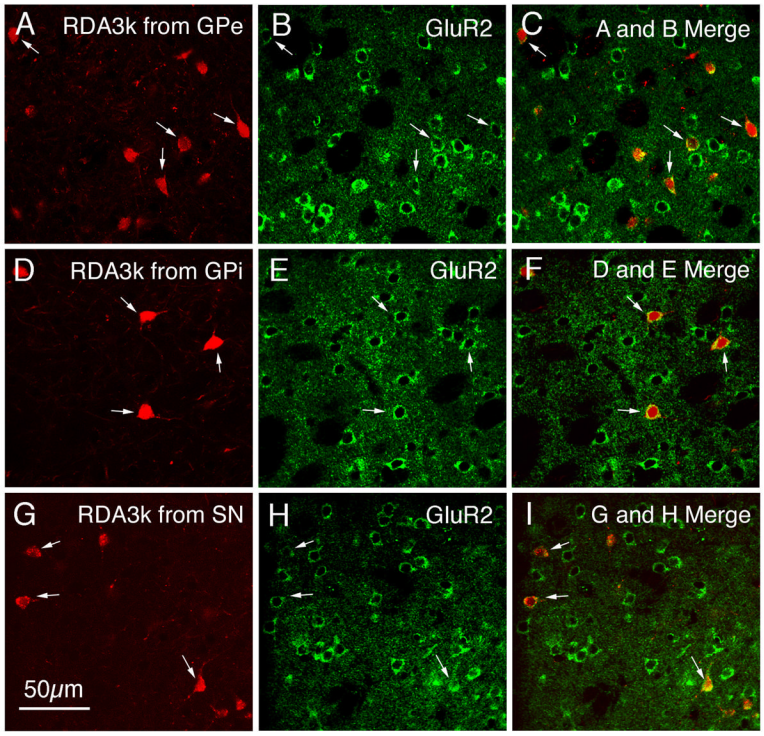

Fig 5.

CLSM images of GluR2 immunofluorescence in neuronal perikarya that had been retrogradely RDA3k-labeled from GPe (A–C), GPi (D–F), and SN (G–I). The GluR2 immunolabeling (B, E, H) was visualized with an Alexa 488 (green), while the neuronal perikarya retrogradely labeled from GPe (A), GPi (D), or SN (G) were labeled with RDA3k (red). Perikaryal double-labeling is evident as a yellow-orange ring (C, F, I), reflecting an overlap of the green cytoplasmic labeling for GluR2 with the red RDA3k in the retrogradely labeled perikarya. Double-labeled neurons are indicated by arrows, and all striatal neurons retrogradely labeled from GPe, GPi, or SN were immunolabeled for GluR2. Magnification is the same in all images. For abbreviations, see list.

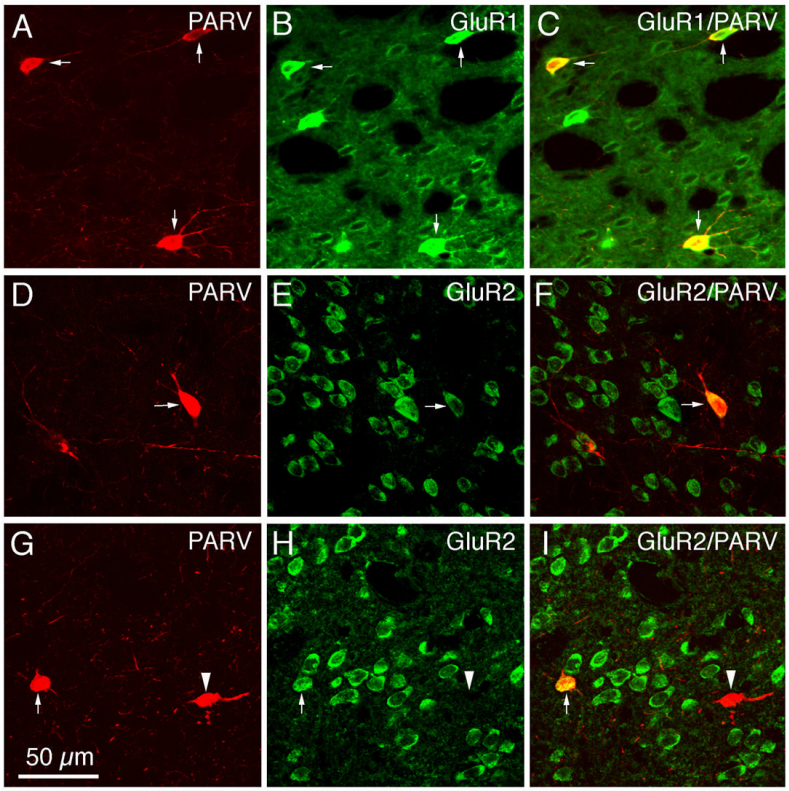

Fig 6.

CLSM images of GluR1 (A–C) or GluR2 (D–I) immunofluorescence in parvalbuminergic (PARV+) striatal interneurons in rat. All PARV+ perikarya were immunolabeled for GluR1, while only some were immunolabeled for GluR2. The GluR1 (B) or GluR2 (E, H) immunofluorescence was visualized with Alexa 488 (green), while the PARV (A, D, G) immunofluorescence was visualized with Alexa 594 (red). Perikaryal double-labeling is evident as a yellow-orange ring (C, F, I), reflecting an overlap of the green cytoplasmic labeling for GluR1 or GluR2 with the red cytoplasmic labeling for PARV. PARV+ perikarya containing GluR1 or GluR2 are indicated by arrows, while PARV+ perikarya lacking GluR2 are indicated by arrowheads. Magnification is the same in all images. For abbreviations, see list.

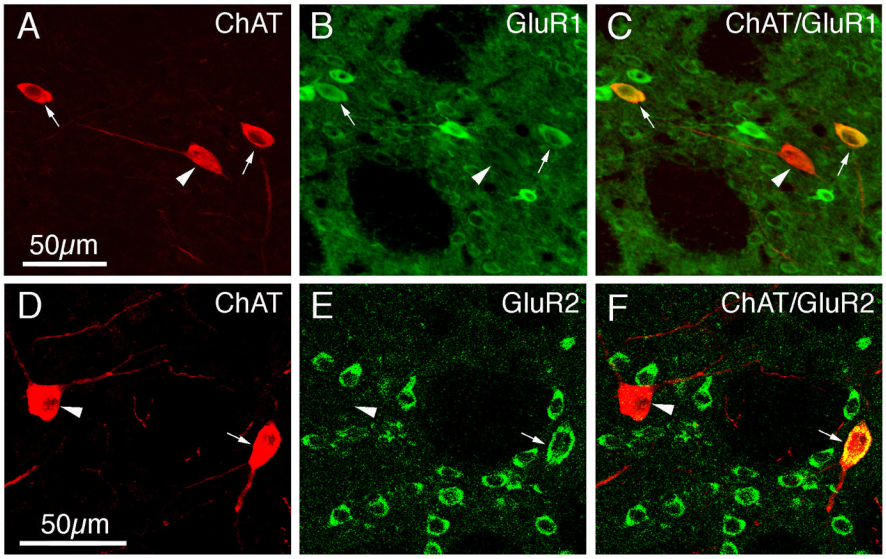

Fig 7.

CLSM images of GluR1 (A–C) or GluR2 (D–F) immunofluorescence in cholinergic choline acetyltransferase-containing (ChAT+) striatal interneurons in rat. The GluR1 (B) or GluR2 (E) immunofluorescence was visualized with Alexa 488 (green), while the ChAT (A, D) immunofluorescence was visualized with Alexa 594 (red). Perikaryal double-labeling is evident as a yellow-orange ring (C, F), reflecting an overlap of the green cytoplasmic labeling for GluR1 or GluR2 with the red cytoplasmic labeling for ChAT. ChAT+ neurons containing GluR1 or GluR2 are indicated by arrows, while ChAT+ neurons not containing GluR1 or GluR2 are indicated by arrowheads. Magnification in B and C same as in A; magnification in E and F same as in D. For abbreviations, see list.

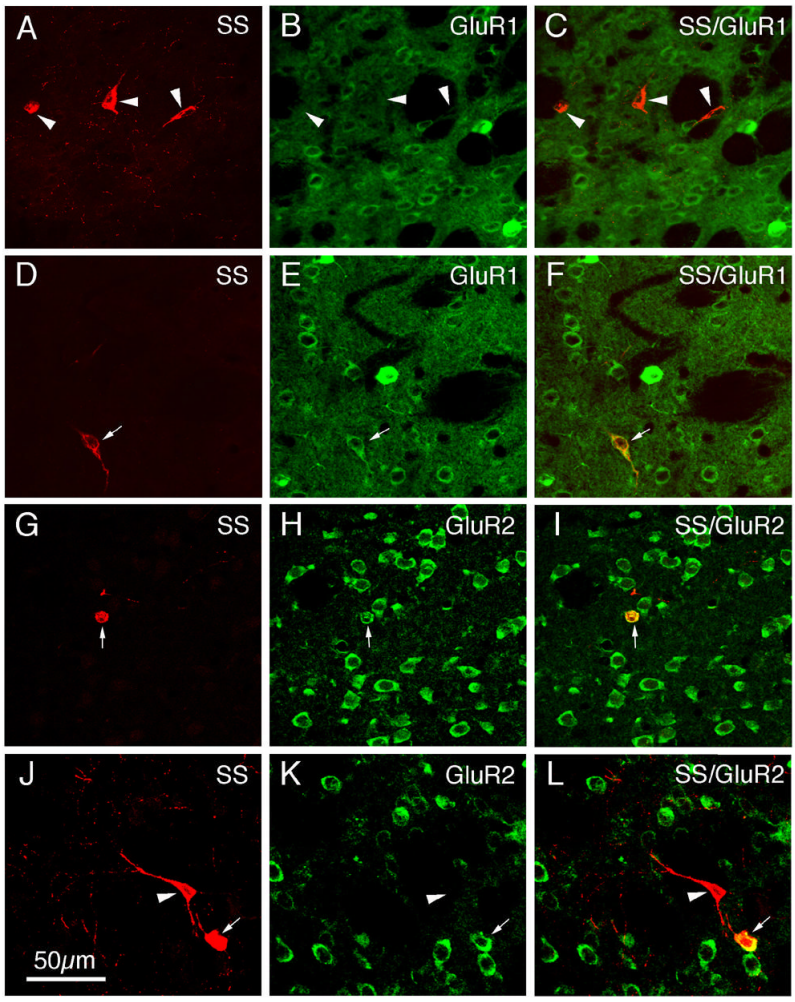

Fig 8.

CLSM images of GluR1 (A–F) or GluR2 (G–L) immunofluorescence in somatostatinergic (SS +) striatal interneurons in rat. The GluR1 (B, E) or GluR2 (H, K) immunofluorescence was visualized with Alexa 488 (green), while the SS (A, D, G, J) immunofluorescence was visualized with Alexa 594 (red). Perikaryal double-labeling is evident as a yellow-orange ring (F, I, L), reflecting an overlap of the green cytoplasmic labeling for GluR1 or GluR2 with the red cytoplasmic labeling for SS. SS+ perikarya containing GluR1 or GluR2 are indicated by arrows, while SS+ perikarya lacking GluR1 or GluR2 are indicated by arrowheads. Magnification is the same in all images. For abbreviations, see list.

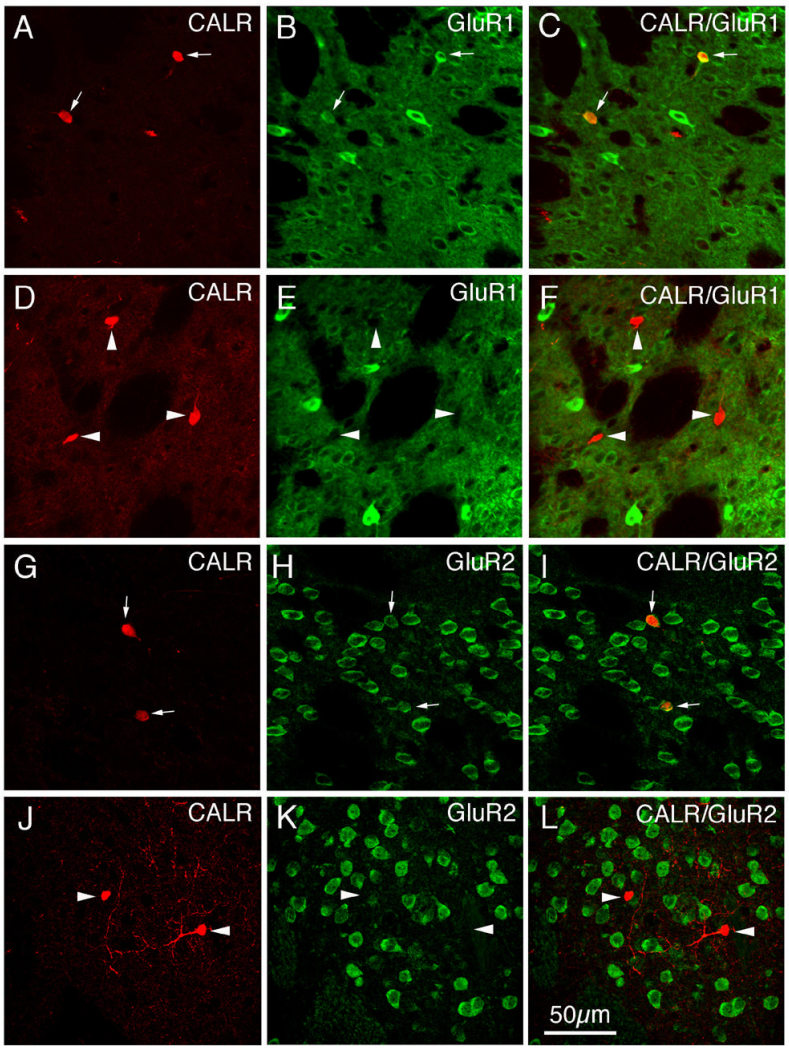

Fig 9.

CLSM images of GluR1 (A–F) or GluR2 (G–L) immunofluorescence in calretinergic (CALR +) striatal interneurons in rat. The GluR1 (B, E) or GluR2 (H, K) immunofluorescence was visualized with Alexa 488 (green), while the CALR (A, D, G, J) immunofluorescence was visualized with Alexa 594 (red). Perikaryal double-labeling is evident as a yellow-orange ring (C, I), reflecting an overlap of the green cytoplasmic labeling for GluR1 or GluR2 with the red cytoplasmic labeling for CALR. CALR+ neurons containing GluR1 or GluR2 are indicated by arrows, while CALR+ neurons lacking GluR1 or GluR2 are indicated by arrowheads. Magnification is the same in all images. For abbreviations, see list.

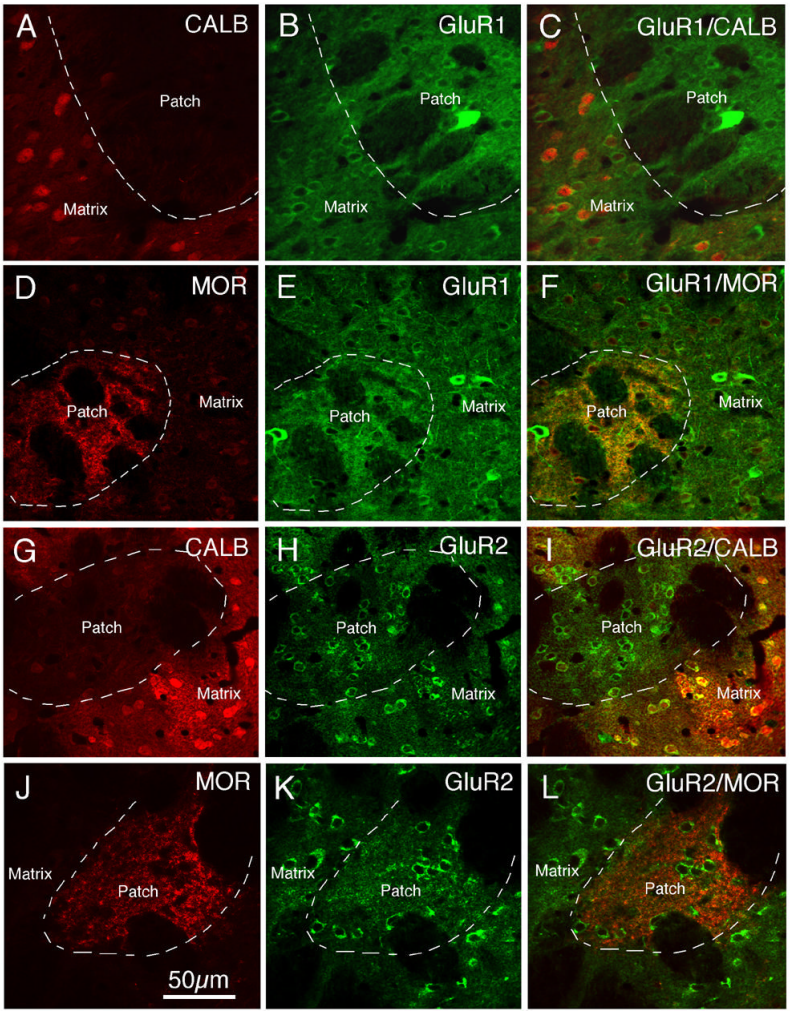

Fig 10.

CLSM images showing GluR1 (A–F) or GluR2 (G–L) immunofluorescence in patch and matrix striatal compartments identified by immunolabeling for CALB (A–C, G–I) or mu opiate receptor (MOR) (D–F, J–L). The images show that GluR1 immunolabeling (visualized with Alexa 488) in the CALB-negative or MOR+ patch compartment (visualized with Alexa 594) is more intense than in the CALB-positive or MOR-negative matrix compartment, while GluR2 immunolabeling (visualized with Alexa 488) in the CALB-negative or MOR positive patch compartment (visualized with Alexa 594) resembles that in the CALB-positive or MOR-negative matrix compartment. Magnification is the same in all images. For abbreviations, see list.

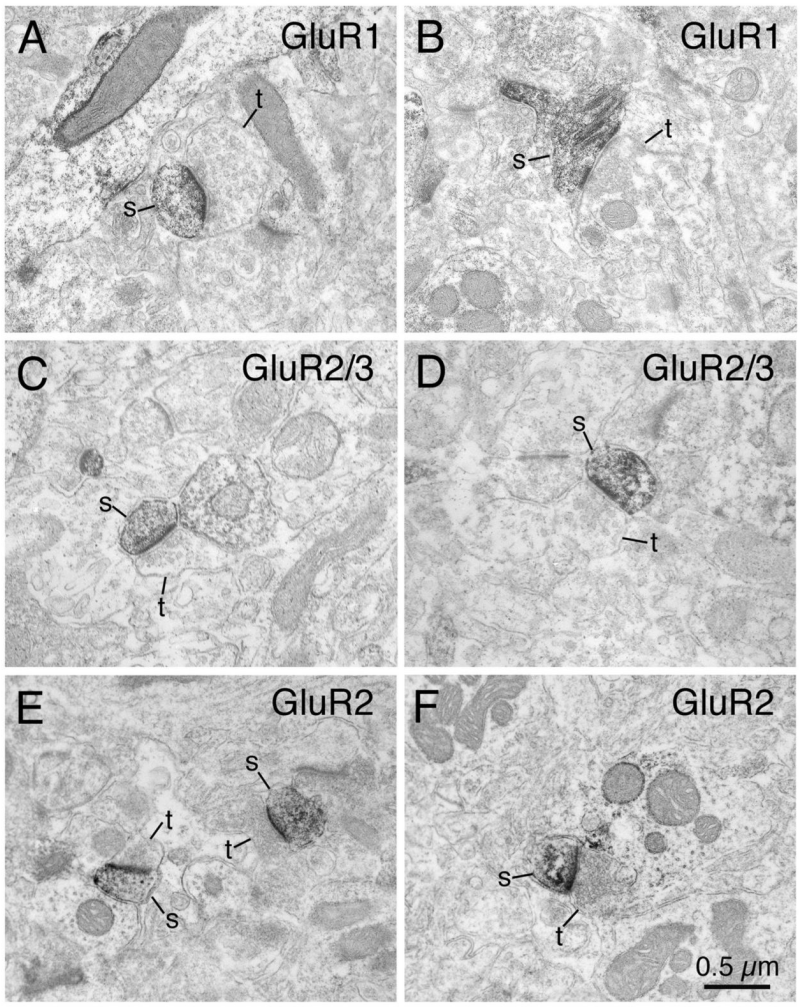

Fig 11.

Electron microscopic images of immunolabeling of rat striatum for GluR1 (A, B), GluR2/3 (C, D), or GluR2 (E, F). Note that GluR1-immunolabeled spines (s) receive asymmetric synaptic contact from large unlabeled terminals (t), while GluR2/3 or GluR2-immunolabeled spines receive asymmetric synaptic contact from smaller unlabeled terminals. Magnification is the same in all images. For abbreviations, see list.

Table 1

Information on the Primary Antibodies Used

Information on the primary antibodies used in the present study, with their dilutions, animal host, supplier, and key references indicating antibody specificity.

Antibody	Dilution	Animal source	Company	References
GluR1	1-3μg/ml	rabbit	Chemicon International Inc., Temecula, CA	Patralia and Wenthold, 1992
GluR2/3	1-3μg/ml	rabbit	Chemicon International Inc., Temecula, CA	Wenthold et al., 1992
GluR2	1-3μg/ml	mouse	Chemicon International Inc., Temecula, CA	Vissavajjhala et al., 1996
CALB	1:500	mouse	Sigma-Aldrich, St. Louis, MO	Celio et al., 1990
CALB	1:500	rabbit	Sigma-Aldrich, St. Louis, MO	Celio, 1990
PARV	1:500	mouse	Sigma-Aldrich, St. Louis, MO	Celio et al., 1988
PARV	1:500	rabbit	DiaSorin, Stillwater, MN	Kagi et al., 1987
ChAT	1:100	goat	Chemicon International Inc., Temecula, CA	Shiromani et al., 1987
ChAT	1:100	rabbit	Chemicon International Inc., Temecula, CA	Bruce et al., 1985
SS	1:100	mouse	Drs. J.C. Brown & S.R. Vincent, Vancouver, BC, Canada	Vincent et al., 1983
SS	1:500	rabbit	ImmunoStar Inc, Hudson, WI	Hendry et al., 1984
CALR	1:1000	mouse	Swant, Bellinzona, Switzerland	Zimmermann and Schwaller, 2002
CALR	1:1000	rabbit	Swant, Bellinzona, Switzerland	Schwaller et al., 1993
MOR	1:1000	guinea pig	Neuromics, Minneapolis, MN	Arvidsson et al., 1995
MOR	1:1000	rabbit	ImmunoStar Inc, Hudson, WI	Wang and Pickel, 1998

CALB, calbindin; PARV, parvalbumin; ChAT, choline acetyltransferase; SS, somatostatin; CALR, calretinin; MOR, mu opiate receptor.

Table 2

GluR1 and GluR2 Frequency in Striatal Neuron Types

Frequency of GluR1 (for 4 rats) and GluR2 (for 5 rats) in the perikarya of each of the main striatal neuron types, as identified by immunolabeling, expressed as the mean ± SEM for the animals studied. The number of neurons of each type on which the percent frequency is based is shown in parentheses for each neuron type.

Subunit	CALB+ Perikarya	PARV+ Perikarya	ChAT+ Perikarya	SS+ Perikarya	CALR+ Perikarya
% with GluR1 (n=4)	61.9% ±1.2 (n=834/1348)	100.0% ±0.0 (n=1691/1691)	68.9% ±9.5 (n=155/223)	14.8% ±5.8 (n=22/156)	51.2% ±9.2 (n=97/205)
% with GluR2 (n=5)	100.0% ±0.0 (n=4800/4800)	73.2% ±6.2 (n=1687/2364)	55.4% ±3.7 (n=1117/2019)	51.8% ±2.2 (n=745/1483)	33.0% ±4.4 (n=210/663)

Table 3

GluR1 and GluR2 Frequency in Striatal Projection Neuron Types

Frequency of GluR1 and GluR2 in the perikarya of each of the striatal projection neuron types, as identified by retrograde RDA3k labeling, expressed as the mean ± SEM for the animals studied. The number of neurons of each type on which the percent frequency is based is shown in parentheses for each neuron type.

Subunit	Striatal Perikarya Retrogradely Labeled from GPe (n=4)	Striatal Perikarya Retrogradely Labeled from GPi (n=4)	Striatal Perikarya Retrogradely Labeled from SN (n=4)
% with GluR1	71.6% ±1.1 (n=280/395)	53.4% ±0.9 (n=123/231)	62.2% ±1.8 (n=171/275)
% with GluR2	100.0% ±0.0 (n=400/400)	100.0% ±0.0 (n=400/400)	100.0% ±0.0 (n=400/400)

Table 4

Intensity of GluR 1 and GluR2 in Striatal Neuron Types

GluR1 and GluR2 immunofluorescence intensity in striatal projection neuron perikarya (CALB+) and interneuron perikarya (ChAT+, PARV+, SS+, CALR +), as measured by image analysis, using a 0 (black) to 255 (white) optical density scale. Mean GluR1 and GluR2 intensities (±SEM) are presented for GluR1-immunolabeled and GluR2-immunolabeled perikarya of each type, as well as for all cells of each type (including those labeled for GluR1 or GluR2 and those not labeled for GluR). The number of neurons of each type on which the mean intensity is based is shown in parentheses for each neuron type. The rank order (by Fisher's PLSD) for GluR intensity for each neuron type (by each of the two grouping approaches) is shown below the table. Higher numbers indicate higher labeling intensity.

Assessment Grouping	CALB+ Perikaryal GluR Intensity	PARV+ Perikaryal GluR Intensity	ChAT+ Perikaryal GluR Intensity	SS+ Perikaryal GluR Intensity	CALR+ Perikaryal GluR Intensity
GluR1 Intensity in Cytoplasm of Cell Body – GluR1+ cells only	43.6 ±2.5 (n=100)	146.5 ±2.9 (n=100)	79.6 ±3.4 (n=100)	46.2 ±3.3 (n=20)	89.4 ±4.6 (n=96)
GluR1 Intensity in Cytoplasm of Cell Body – all cells of type	26.9 ±2.3 (n=162)	146.5 ±2.9 (n=100)	54.9 ±3.9 (n=145)	6.8 ±1.5 (n=136)	45.6 ±4.0 (n=188)
GluR2 Intensity in Cytoplasm of Cell Body – GluR2+ cells only	116.8 ±3.4 (n=100)	113.0 ±3.1 (n=100)	83.4 ±5.1 (n=50)	105.1 ±4.7 (n=50)	85.8 ±5.6 (n=50)
GluR2 Intensity in Cytoplasm of Cell Body – all cells of type	116.8 ±3.4 (n=100)	82.5 ±4.9 (n=137)	46.3 ±5.2 (n=90)	54.2 ±5.9 (n=97)	28.2 ±3.8 (n=152)

by Fisher's PLSD:

For GluR1, GluR1+ cells of type only: PARV>CALR>ChAT>CALB=SS

For GluR1, all cells of type: PARV>ChAT>CALR>CALB>SS

For GluR2, GluR2+ cells of type only: CALB=PARV=SS>CALR=ChAT (but CALB>SS)

For GluR2, all cells of type: CALB>PARV>ChAT=SS>CALR

inferred GluR1:GluR2 ratio for all striatal neurons: PARV>CALR>ChAT>CALB>SS

Table 5

Intensity of GluR 1 and GluR2 in Striatal Projection Neurons Types

GluR1 and GluR2 immunostaining intensity in striatal projection neuron perikarya identified by retrograde labeling from GPe, GPi or substantia nigra, as measured by image analysis using a 0 (black) to 255 (white) optical density scale. Higher values indicate higher labeling intensity.

Assessment Grouping	Striatal Perikarya retrogradely labeled from GPe	Striatal Perikarya retrogradely labeled from GPi	Striatal Perikarya retrogradely labeled from SN
GluR1 Intensity in Cytoplasm of Cell Body – GluR1+ cells only	57.6 ±2.3 (n=100)	41.8 ±2.1 (n=100)	47.1 ±2.1 (n=100)
GluR1 Intensity in Cytoplasm of Cell Body – all cells of type	40.9 ±2.8 (n=141)	22.1 ±1.9 (n=188)	29.2 ±2.2 (n=161)
GluR2 Intensity in Cytoplasm of Cell Body – GluR2+ cells only	88.5 ±2.3 (n=120)	98.9 ±2.5 (n=120)	90.3 ±2.4 (n=120)
GluR2 Intensity in Cytoplasm of Cell Body – all cells of type	88.5 ±2.3 (n=120)	98.9 ±2.5 (n=120)	90.3 ±2.4 (n=120)

by Fisher's PLSD:

For GluR1, GluR1+ cells of type only: striato-GPe=striatonigral>striato-GPi

For GluR1, all cells of type: striato-GPe>striatonigral>striato-GPi

For GluR2, GluR2+ cells of type only: striato-GPi>striatonigral=striato-GPe

For GluR2, all cells of type: striato-GPi>striatonigral=striato-GPe

inferred GluR1:GluR2 ratio for all projection neurons: striato-GPe>striatonigral>striato-GPi

Table 6

GluR1 and GluR2 Intensity in Patch versus Matrix Neurons

GluR1 and GluR2 immunostaining intensity in patch versus matrix compartment neuronal perikarya, as measured by image analysis using a 0 (black) to 255 (white) optical density scale. The patch compartment was defined by CALB-negative or mu opiate receptor-rich (MOR+) immunolabeling, while the matrix compartment was defined by CALB-rich or MOR- poor immunolabeling. Mean GluR1 and GluR2 intensities (±SEM) are presented for GluR1+ or GluR2+ perikarya of each compartment. The number of neurons of each type on which the mean intensity is based is shown in parentheses for each neuron type. The rank order (by Fisher's PLSD) for GluR intensity for each compartment is shown below the table. Higher numbers indicate higher labeling intensity.

Assessment Grouping	CALB− Patch	CALB+ Matrix	MOR+ Patch	MOR− Matrix
GluR1 Intensity in Cytoplasm of Cell Body – GluR1+ cells only	62.1 ±2.6 (n=100)	44.2 ±2.3 (n=100)	61.7 ±3.3 (n=50)	47.3 ±3.5 (n=50)
GluR2 Intensity in Cytoplasm of Cell Body – GluR2+ cells only	108.1 ±3.5 (n=100)	116.8 ±3.4 (n=100)	97.6 ±2.5 (n=50)	101.4 ±3.1 (n=50)

by Fisher's PLSD:

For GluR1, patch>matrix

For GluR2, patch=matrix

inferred GluR1:GluR2 ratio for projection neurons: patch>matrix

Table 7

Ultrastructural Localization of GluR1, GluR2/3 and GluR2

Ultrastructural localization of GluR1, GluR2/3, and GluR2 in rat striatum. The frequencies of striatal spines and dendrites immunolabeled for GluR1, GluR2/3, and GluR2 were determined from electron microscopic (EM) images. The sizes of asymmetric axodendritic or axospinous synaptic terminals received by GluR1, GluR2/3, or GluR2 spines and dendrites were measured on the EM images. The number of spines or dendrites of each type on which the mean frequencies (±SEM) are based is shown in parentheses for each structure type.

Subunit	Percent of Striatal Dendrites Immunolabeled for the GluR	Percent of Striatal Spines Immunolabeled for the GluR	Size of Asymmetric Axodendritic Synaptic Terminals Received by GluR+ Dendrites	Size of Asymmetric Axospinous Synaptic Terminals Received by GluR+ Spines
GluR1	60.8% (647/1064)	53.3% (631/1184)	0.642μm ±0.040 (n=46)	0.614μm ±0.030 (n=432)
GluR2/3	66.3% (961/1450)	66.0% (805/1220)	0.455μm ±0.018 (n=73)	0.438μm ±0.014 (n=418)
GluR2	41.8% (610/1460)	39.9% (558/1399)	0.423μm ±0.028 (n=78)	0.417μm ±0.006 (n=563)